

ATMOSPHERIC HORIZONTAL UNIFORMITY
MEASURED BY A STEERABLE LASER
SYSTEM AT THE HIGH
RESOLUTION FLY'S
EYE

Jonathan Reid Mumford

A Senior Honors Thesis submitted to the faculty of

The University of Utah

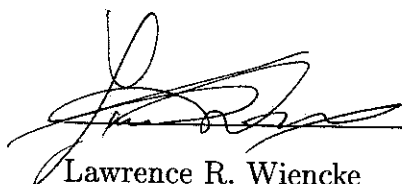
In partial fulfillment of the requirements for the

Honors Degree of Bachelor of Science

In

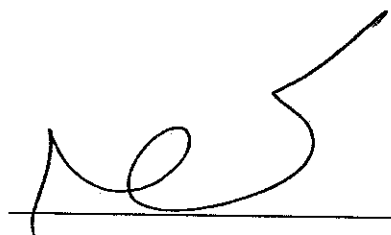
Physics

APPROVED:



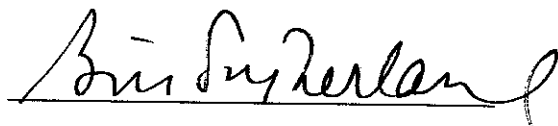
Lawrence R. Wiencke

Supervisor



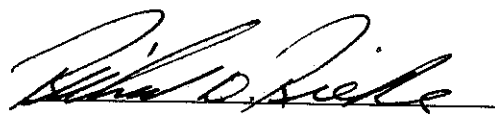
Z. Vally Vardeny

Chair, Physics



Bill Sutherland

Departmental Honors Advisor



Richard D. Rieke

Director, Honors Program

August 2000

ABSTRACT

The optical horizontal uniformity of the atmosphere surrounding the HiRes cosmic ray detector is measured using a steerable laser system (HR2SLS). Most models assume horizontal uniformity to achieve a one dimensional characterization of the atmosphere. The validity of this assumption is discussed. Possible asymmetries in the HiRes detector and HR2SLS are discussed. A method is developed whereby one can identify asymmetries in the atmosphere without being certain of the absolute calibration of the HiRes detector. At small scales, the atmosphere appears to be uniform but begins to show asymmetries at large distances.

TABLE OF CONTENTS

ABSTRACT	ii
TABLE OF CONTENTS	iii
LIST OF FIGURES	x
LIST OF TABLES	x
1 INTRODUCTION	1
2 ATMOSPHERIC MODELS	3
3 THE APPARATUS	7
3.1 THE HIRES 1 DETECTOR	7
3.2 THE HIRES 2 STEERABLE LASER SYSTEM	9
4 THE DATA SET	14
5 APPARATUS ASYMMETRIES	17
5.1 POSSIBLE LASER ASYMMETRIES	17
5.1.1 ENERGY AS A FUNCTION OF POINTING DIRECTION .	18
5.1.2 POLARIZATION EFFECTS	18
5.1.3 LASER ENERGY JITTER	20
5.1.4 LASER POINTING ACCURACY	22
5.2 POSSIBLE DETECTOR ASYMMETRIES	23
5.2.1 DETECTOR GEOMETRY	23
5.2.2 ABSOLUTE CALIBRATION	25
5.2.3 RELATIVE CALIBRATION	30

6	ATMOSPHERIC ASYMMETRIES	32
6.1	MOLECULAR ASYMMETRIES	32
6.2	METEOROLOGICAL ASYMMETRIES	32
6.3	\mathcal{R} -PLOTS	33
6.4	AEROSOL ASYMMETRIES	36
6.5	TRENDS IN ASYMMETRY	44
7	CONCLUSION	53
A	\mathcal{R}-PLOTS FOR SEPTEMBER 7, 1999	55
B	AUTOMATIC LASER SUMMARY REPORTS	67

LIST OF FIGURES

1	A map of the West desert of Utah. The locations of both the HiRes 1 and HiRes 2 detectors are shown. The steerable laser is located at the site of the HiRes 2 detector. The detector is located on a small ridge that overlooks a valley to the West. If one draws an imaginary line between the two detector sites, it is clear that the ground topology is not symmetric on either side.	2
2	A comparison of Aerosol and Molecular phase functions.	5
3	One of the mirrors that make up the HiRes detector. Each mirror images light from the night sky onto a "camera" of 256 hexagonal photo-multiplier tubes that take snapshots of the light fluctuations.	8
4	Schematic diagram of the HR2SLS.	10
5	Photograph of the optical elements of the HR2SLS. In the foreground, one can see the monitor probe used to measure the laser energy reflected from the beam splitter. On the right are two computer controlled filter wheels that are preceded, on the left, by a $\frac{1}{4}$ -wave plate to produce circularly polarized light.	12
6	Photograph of the laser steering head. The HiRes detector is located on the hill in the distance directly above the near corner of the steering head. . .	13
7	Laser geometries used in this study. The figure shows laser shots taken with zenith angles of 10° . Tracks in red are those tracks that were used in this study. Another set of shots, with elevation angles of 15° and the same azimuthal geometries as pictured above, were also used in this study. The inset box shows a closeup of the HiRes detector. Small circles represent mirror locations. Shots taken at a zenith angle of 0.6° and 2° either side of the detector are shown.	16

8	Light emitted from the HR2SLS as a function of pointing direction. The upper box shows the relative intensity as a function of azimuthal angle for a zenith angle of 15° . The lower box shows a similar plot for a zenith angle of 0° . The intensity never varies by more than about 3% over the entire range of azimuthal angles.	19
9	Comparison of laser energy from different shots over a five minute period. The top panel shows groups of shots that were taken at different laser geometries. Two of the positions are compared in the histograms below. The average laser energy for two shot geometries differs by approximately 3.5%. The analysis includes a correction for this effect.	21
10	Laser shots taken at 319° azimuth and 10° elevation. The top laser shot was taken in September, 1999 while the lower was taken in January of 2000. According to an amplitude weighted plane fit, the pointing direction of the two tracks differs by approximately 0.193°	24
11	A map of the HiRes detector.	25
12	Profiles of Monte Carlo simulated laser shots, with a geometry of 36° azimuth and 0.6° zenith, in four different atmospheres. The open circles are for a molecular atmosphere. Atmospheres with aerosol extinction lengths of 25 km, 9 km, and 6.5 km are shown by black, red, and blue markers respectively.	28
13	A comparison of data calibrated using both the old and new methods, shown by black and blue markers respectively, for a laser shot at 0.6° zenith and 36° azimuth. A Monte Carlo prediction for an aerosol extinction length of 9.0 km is superimposed in red.	29

14	Plot of ratios for data taken on the 8th of January, 2000. Notice the deviation from one in the \mathcal{R} -plot (bottom right panel) indicating that more light was measured on the South side of the detector than on the North.	34
15	The top panel shows the North track (azimuth= 109°) being obscured by a cloud. The bottom panel shows the symmetric track on the South side of the detector (azimuth= 319°). This track was not impeded by cloud cover and is detected by several more mirrors. Both laser shots were taken during the same hour and have the same zenith angle of 10°	35
16	Data taken on September 7, 1999. The atmosphere has a high concentration of aerosols shown by the sharp peak in the upper two right panels. The laser shots shown pass very near the detector (azimuth angles of 36° and 32° at 0.6° elevation). At small distances, the atmosphere appears to be uniform.	37
17	Data taken on September 7, 1999. Azimuth angles of 79° and 349° are shown. Both shots have elevation angles of 10° . The atmosphere has a high concentration of aerosols. There is a "hole" in the track at 349° because a mirror of the HiRes detector was not run this evening. The \mathcal{R} -plot shows that there is a large atmospheric asymmetry measured between the two sides of the detector. In this case, the Southern track is significantly dimmer than the Northern track.	39

18	<p>Each row shows \mathcal{R}-plots from a given hour. The laser geometry shown is 79° and 349° azimuth and 10° zenith. Beginning in UT hour 6, the asymmetry is measured at distances greater than 20 km. By hour 7, the asymmetry has moved closer and is now observed at distances greater than 18 km. In UT hour 8, the asymmetry is observed at distances that are less than 20 km. The asymmetry continues to move until it has mostly passed by hour 9. Laser profiles, shown in appendix A, demonstrate that most of the measured asymmetry comes from changes in the North track.</p>	40
19	<p>Data taken on September 9, 1999. The atmosphere has a much lower aerosol concentration compared to September 7. The asymmetry measured on September 7, 1999 (figure 17) is gone. The number of photons measured on either side of the detector, now agree with the measurements made on the reference day. The optical clarity of the atmosphere is symmetric. . . .</p>	41
20	<p>Monte Carlo data generated to replicate the asymmetry measured on September 7, 1999. The North track was generated using an aerosol extinction length of 12 km while the South was generated with 9 km. The extinction length difference produces an asymmetry that appears to be consistent with that measured on September 7, 1999.</p>	43
21	<p>September data: Laser shots 2° either side of the detector are pictured in the first panel. The other three panels show shots taken at a zenith angle of 15°. The laser geometry is listed below each panel. Notice that the RMS deviation tends to increase as one moves further from the detector. All means are close to 1, suggesting a symmetric atmosphere.</p>	45

22	September data: Laser geometry is listed below each panel. This page shows shots that were taken at 10° elevation. Notice that the RMS deviation for these lower shots is greater than the corresponding deviation for the 15° elevation shots pictured on the previous page suggesting the presence of low-elevation asymmetric aerosols.	46
23	October data: Laser geometry is listed below each panel. Again, it appears that the RMS deviation increases as one moves further from the detector. .	47
24	October data: Laser geometry is listed below each panel. Notice that the RMS deviation for the shots at 15° (previous page) are smaller than those for 10° (this page). This may indicate that there were high clouds scattering the shots with greater elevation angles.	48
25	December data: Laser geometry is listed below each panel. The mean of the shots made at ±2° of the detector appears to have shifted indicating an asymmetry. In this case the South side of the detector measured a brighter signal than the North side when compared to the reference day. This is almost certainly not an atmospheric effect since the distance scale is so small. The reference day used to compare the data is from September. This offset mean may be an indication that the detector response changed between September and December.	49
26	December data: Laser geometry is listed below each panel.	50
27	January data: Laser geometry is listed below each panel. Again, the ±2° distribution appears to show an asymmetry.	51
28	January data: Laser geometry is listed below each panel. These distributions suggest that January had one of the more symmetric atmospheres (at least for low elevations) in this data set.	52
29	September 7, 1999; 6:00 UT. Azimuth angles of 36° and 32° at 0.6° elevation.	56

30	September 7, 1999; 7:00 UT. Azimuth angles of 36° and 32° at 0.6° elevation.	57
31	September 7, 1999; 8:00 UT. Azimuth angles of 36° and 32° at 0.6° elevation.	58
32	September 7, 1999; 6:00 UT. Azimuth angles of 79° and 349° at 10° elevation.	59
33	September 7, 1999; 7:00 UT. Azimuth angles of 79° and 349° at 10° elevation.	60
34	September 7, 1999; 8:00 UT. Azimuth angles of 79° and 349° at 10° elevation.	61
35	September 7, 1999; 9:00 UT. Azimuth angles of 79° and 349° at 10° elevation.	62
36	September 7, 1999; 6:00 UT. Azimuth angles of 124° and 304° at 15° elevation.	63
37	September 7, 1999; 7:00 UT. Azimuth angles of 124° and 304° at 15° elevation.	64
38	September 7, 1999; 8:00 UT. Azimuth angles of 124° and 304° at 15° elevation.	65
39	September 7, 1999; 9:00 UT. Azimuth angles of 124° and 304° at 15° elevation.	66
40	Sample automatic summary report.	69
41	Monitor probe energy as a function of UT hour.	70
42	Total average laser energy plotted versus Julian day. Although the laser energy is dropping, it appears to be stabilizing since it was reinstalled in December 1999 (around Julian day 10940).	71
43	Plots that monitor the performance of the laser over different energy regions.	73
44	Commands issued by the operator during the night of laser operation. . .	75

LIST OF TABLES

1	Specifications of the HiRes 2 Steerable Laser System	11
2	Summary laser data sample.	14
3	The relative position of each mirror in the HiRes 1 detector. All measures are in meters	26

1 INTRODUCTION

The High Resolution Fly's Eye (HiRes 1) cosmic ray detector observes cosmic rays in a volume of approximately 6500 cubic kilometers. The detector measures ultra-violet light produced when cosmic rays enter the earth's atmosphere. The HiRes detector is located in the West Desert of Utah where the air is generally clear and dry. However, the clarity of the atmosphere is susceptible to changing factors in the environment such as wind, cloud cover, and pollution. To accurately measure high-energy cosmic rays, one must understand the effect of the atmosphere on light that has propagated from a shower to the detector.

The HiRes 2 Steerable Laser System (HR2SLS), has been installed at Camel's Back Ridge, Dugway Utah to provide atmospheric monitoring for the HiRes detector. The laser is located approximately 12.6 kilometers from the HiRes detector. The laser is used to "probe" the atmosphere in the neighborhood of the HiRes detector. Light scattered from the pulsed, 355nm, beam is measured by the HiRes detector. From the measured signal, one can study the optical characteristics of the atmosphere.

Although the HiRes detector was constructed to measure cosmic rays of the highest energies, the unique design and configuration of the laser and detector, make it a powerful instrument for studying the atmosphere. Modeling the atmosphere is a complicated problem. In order to simplify the model one generally assumes that the atmosphere is horizontally uniform. The atmosphere can then be described in terms of parameters that only change with elevation.

This technique simplifies the model significantly but it completely ignores any effect that ground topology might have on atmospheric clarity. A topological map of the HiRes detector shows that the surroundings are not horizontally symmetric. It is reasonable to imagine aerosol distributions changing depending on the ground

topology. For example, the concentration of aerosols in valleys might be higher than above mountains.

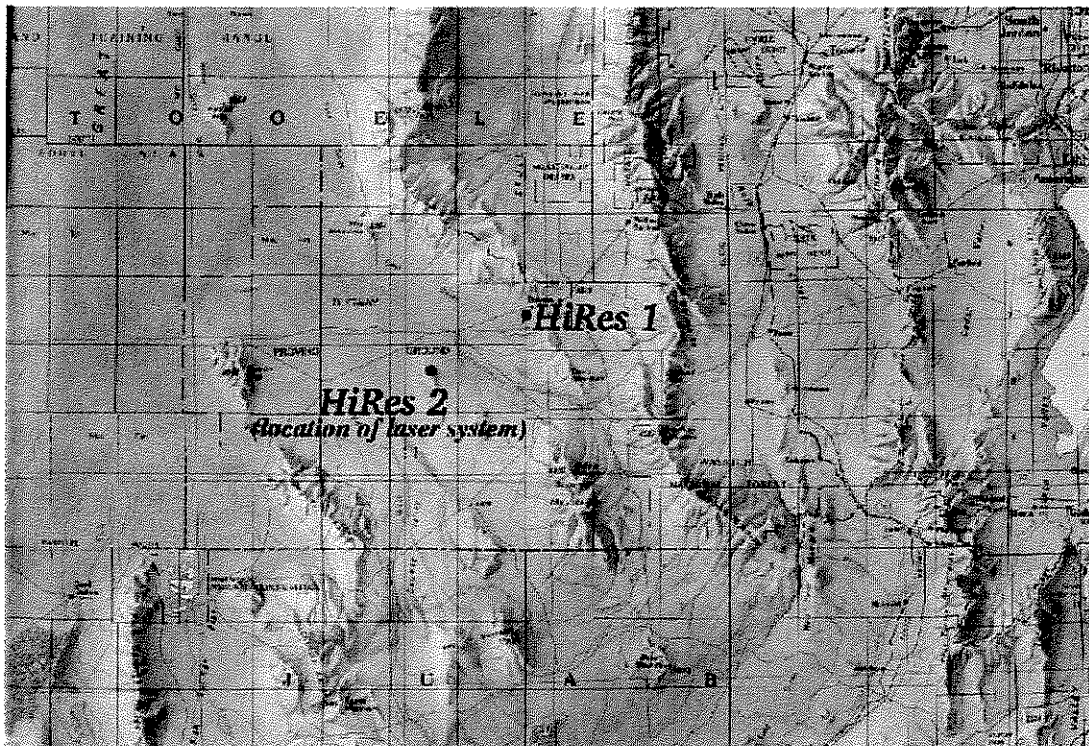


Figure 1: A map of the West desert of Utah. The locations of both the HiRes 1 and HiRes 2 detectors are shown. The steerable laser is located at the site of the HiRes 2 detector. The detector is located on a small ridge that overlooks a valley to the West. If one draws an imaginary line between the two detector sites, it is clear that the ground topology is not symmetric on either side.

This paper will discuss measurements made by HiRes 1 of laser shots from HR2SLS that monitor the clarity of the atmosphere. Horizontal symmetry of the atmosphere will be tested by comparing symmetric laser shots either side of the HiRes detector.

2 ATMOSPHERIC MODELS

The complexity and chaotic nature of the atmosphere make it an impossible system to describe exactly. Several models have been developed that are used to approximate the optical characteristics of the atmosphere. A popular method for modeling the atmosphere is to divide it into horizontal layers that exhibit unique optical characteristics. Distinct layers in the atmosphere may be described qualitatively as follows[1].

Boundary or Mixing Layer: is generally the lowest kilometer of the atmosphere.

The boundary layer is the most volatile region due to its close proximity with the surface of the earth. The boundary layer picks up heat, moisture, aerosols, and radiation from the surface. The heated air becomes buoyant and rises forming many turbulent pockets in this region. The turbulence in the mixing layer provides a mechanism for picking up surface particles and depositing them in the atmosphere.

Troposphere: is typically the lowest 10 kilometers of the atmosphere. The troposphere is bounded above by the tropopause, an isothermal layer that acts as a barrier to convection currents in the troposphere. Convection dominates the dynamics of the troposphere, causing warm air, heated at the surface, to rise. Water vapor in the troposphere interacts with the energy from the heated air pockets to form clouds. Much of the meteorology that we observe takes place in the troposphere.

Stratosphere: is the layer directly above the troposphere. In the stratosphere, the temperature increases with altitude due to the absorption of the Sun's ultraviolet radiation. In the stratosphere, convection is unimportant.

In each of these regions, transmission of light is described by scattering processes. The two most important scattering processes are Rayleigh and Mie scattering.

Rayleigh scattering describes the scattering of electro-magnetic radiation from independent particles much smaller than the wavelength of the incident radiation. For example, ultra-violet light scattered by air molecules. Rayleigh scattering describes the transmission of light in a purely molecular atmosphere. However, if there are aerosols, Mie scattering becomes important. Mie scattering describes the scattering of electro-magnetic radiation from spherical particles whose size is comparable to the wavelength of the incident radiation. In the presence of aerosols, the clarity of the atmosphere is described by a superposition of molecular and aerosol atmospheres described by Rayleigh and Mie scattering respectively.

Molecular and aerosol *phase functions* describe the amount of radiation scattered as a function of scattering angle (see figure 2). The aerosol phase function is *forward peaked*, meaning that light scatters preferentially at small scattering angles. When the aerosol concentration is high, the effect of Mie scattering is much larger than Rayleigh scattering at small scattering angles.

Compared to changes in the molecular density of the atmosphere, changes in aerosol densities are larger and occur on a smaller time scale. Several models have been developed to describe the concentration of aerosols as a function of elevation. These models include the *Wind Dependent Desert Aerosol Model*[2] developed by David R. Longtin and the *Standard Desert Atmosphere*[3] developed by the National Oceanic and Atmospheric Administration (NOAA).

A simple version of the Longtin model describes the distribution of aerosols at a given ground wind speed. When an aerosol distribution is known, one can then model the clarity of the atmosphere in as little as three parameters: the ground level extinction length, the aerosol scale height, and the depth of the mixing layer.

The transmission, T , can be expressed as

$$T(\theta_1, \theta_2, h) = e^{-\frac{h_0}{x} \left(\frac{1}{\sin(\theta_1)} + \frac{1}{\sin(\theta_2)} \right) (1 - e^{h/h_0})} \quad (1)$$

where θ_1 is the zenith angle of the laser, θ_2 is the zenith angle at which the light is observed, x is the horizontal extinction length, and h_0 is the aerosol scale height.

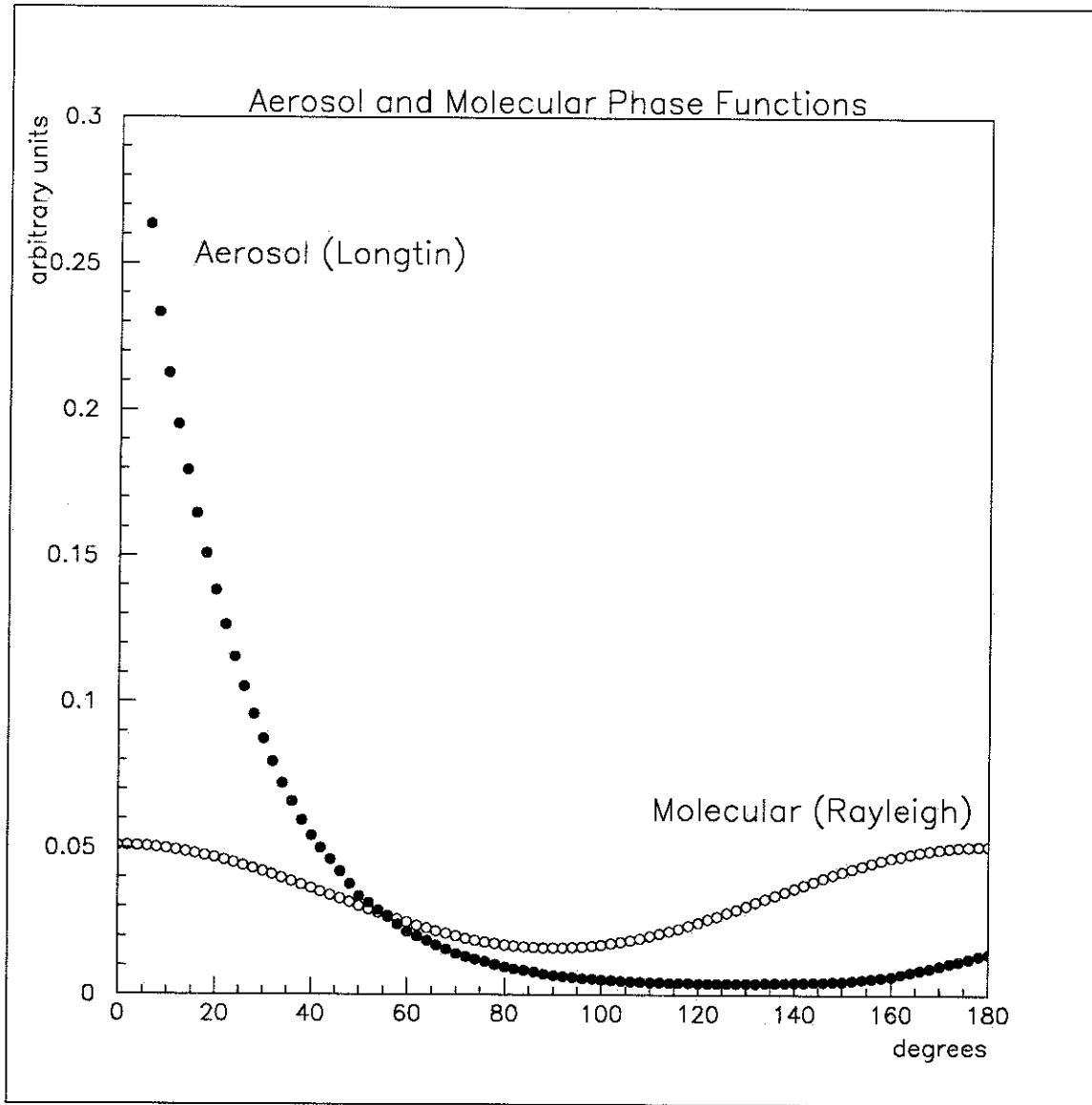


Figure 2: A comparison of Aerosol and Molecular phase functions.

The extinction length is the distance that light must travel before it is attenuated by a factor of e^{-1} . The scale height describes the change in the density of aerosols as a function of elevation. In the simple three-parameter model, aerosol distribution is exponential with height, with large particle densities close to the surface. The mixing layer is the depth of the region, near the ground, where the aerosol content is more dense and considered uniform.

One-dimensional aerosol models depend on the horizontal uniformity of the atmosphere. A horizontal aerosol gradient could be fatal to the predictions of such a model. To first order, modeling the atmosphere as a function of elevation alone makes sense because the gravitational force acting on the atmosphere is uniform. However, if we now consider wind and the local geography in our atmospheric system, does the horizontal symmetry still hold?

3 THE APPARATUS

The HiRes detector uses the atmosphere as a calorimeter to measure radiation from extensive air showers produced when incident cosmic rays interact with the atmosphere. The HiRes detector measures fluctuations in the night sky background in the UV spectrum, namely at the primary nitrogen emission wavelength of $337nm$ [5]. Because the HiRes detector only measures light fluctuations brighter than the night-sky background, the detector is run only during clear, moon-less nights when the background light is minimal.

A laser allows one to monitor a large volume of atmosphere efficiently. The traditional method is to measure light, back-scattered from a laser, with a single detector. This method is called Light Detection And Ranging or LIDAR.

At HiRes, light scattered from a remote laser (HR2SLS) is measured for many different scattering angles simultaneously. This type of LIDAR, where the observer is separated from the light source, is called *Bi-Static LIDAR*. Bi-Static LIDAR is more flexible than other LIDAR systems where only the back-scattered light is measured because one can measure light scattered from the laser at many different scattering angles[6]. A brief description of both the HiRes 1 detector and the HiRes 2 Steerable Laser System follows.

3.1 THE HIRES 1 DETECTOR

The HiRes 1 detector is the first of two detectors that compose the High Resolution Fly's Eye Cosmic Ray Observatory. It is located in the West desert of Utah on the U.S. Army's *Dugway Proving Grounds*. These detectors are built on hills generally above much of the low level aerosols like large dust particles and ground fog. A second detector, HiRes 2, is located approximately 12.6 km from HiRes 1.

The HiRes detector, comprising both the HiRes 1 and 2 sites, is composed of 63 clover-shaped mirrors each with an area of approximately $3.5 m^2$. At the focal plane

of each mirror is a camera of 256 photo-multiplier tubes (PMT). Each PMT views approximately 1° solid angle of sky. The positions and pointing directions of the mirrors and PMT's are fixed. The mirrors are divided between the two sites or eyes. The HiRes 1 eye has 20 mirrors that view nearly 360 degrees in azimuth from 3.5 to 16 degrees in elevation angle. The detector looks close to the horizon; viewing a large volume of atmosphere, to maximize the aperture of the detector.

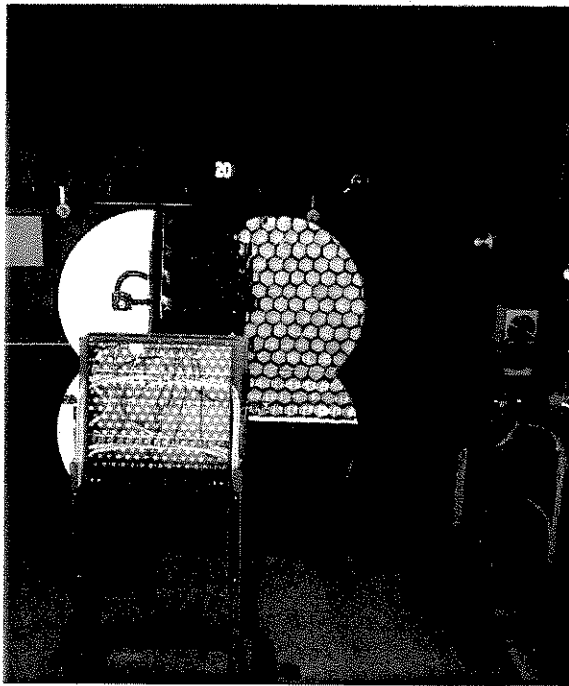


Figure 3: One of the mirrors that make up the HiRes detector. Each mirror images light from the night sky onto a “camera” of 256 hexagonal photo-multiplier tubes that take snapshots of the light fluctuations.

The HiRes detector was constructed to measure Cosmic Rays of the highest energies. However, the large aperture and unique geometry make it a powerful instrument for measuring the optical characteristics of the atmosphere. HiRes has several advantages over other bi-static LIDAR systems. The HiRes detector views almost 360° in azimuth simultaneously. Other systems use only one movable detector. Moreover, the large area of the mirrors composing the HiRes detector makes it possible to measure light scattered from a laser at very large distances. The HiRes detector also uses 5120

PMT's to provide a high resolution picture of measured light. Other LIDAR systems typically use only one photo-tube. These features make the HiRes detector one of the most powerful instruments in the world for measuring the optical clarity of the atmosphere.

3.2 THE HIRES 2 STEERABLE LASER SYSTEM

The HR2SLS uses a 355 *nm*, pulsed YAG laser[7]. Each pulse has a duration of approximately, 5.5 nanoseconds. The laser has been ruggedized for use in field applications. The laser is configured to produce a linearly polarized beam with dichroics to reduce the 512 *nm* and 1024 *nm* harmonics. The laser is mounted to an enclosed optical table that also houses the other optical components of the system. During a typical night of laser operation, the laser runs for between 2 and 10 hours, firing between 2,000 and 13,000 shots. Generally, the laser is fired at a rate of 4 Hz.

1% of the beam is measured by a radiometer and silicon-diode probe to determine the relative energy of each shot. The measured energy is then used by the software to calculate the energy that is shot into the sky (see section 5.1.1).

After being sampled, the beam passes through a quarter wave plate. This wave plate converts the linearly polarized beam from the laser to one that is circularly polarized.

The circularly polarized beam then passes through two computer-controlled filter wheels (see figure 5). The filter wheels allow an operator to vary the intensity of the beam remotely and to choose between circular and two linear polarizations. The filters make it possible to measure light from the laser, without saturating the detector, both close to the HiRes detector and at large distances. Each filter wheel can accommodate eight, one-inch optical elements. The first filter wheel houses one open filter position, one blocked position that is used as a safety precaution, and six neutral density filters with transmission coefficients from 48% to 0.7%. The second filter wheel houses two quarter wave plates (oriented with their retarding axes perpendicular to one another),

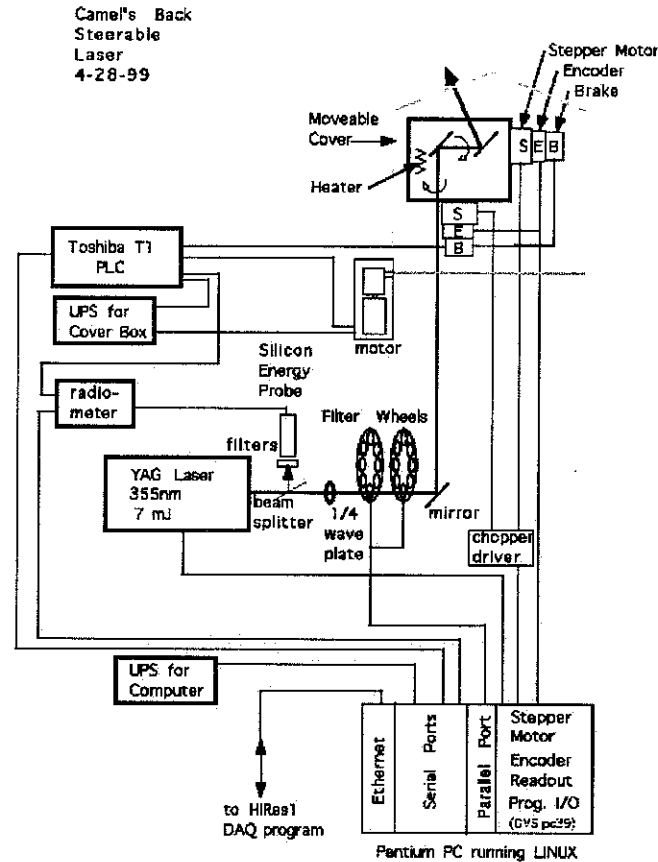


Figure 4: Schematic diagram of the HR2SLS.

four neutral density filters (with transmission coefficients from 48.0% to 12.0%), one open filter position, and another blocked position. The quarter-wave plates have been positioned to give vertically and horizontally polarized light when the beam is aimed towards HiRes 1.

After the beam passes the two filter wheels, it enters a large vertical pipe where it is reflected vertically by a 45° dielectric mirror into the laser steering head (see figure 4).

The laser steering head is a custom-built mechanism that uses two 45° dielectric mirrors, that rotate about the axis of the laser beam, to direct it in any direction

System Function	Specification
Laser, Wavelength	YAG, 355nm
Laser, Pulse Length	5.5 nS
Laser, Energy (to Sky)	7-8mJ (maximum)
Laser, Stability	5% σ
Laser, Divergence	< 0.05°
Filters	48% - 0.08% (24 combinations)
Energy Measurement	1% relative 5% absolute
Polarization Options	Circular, Linear (H or V)
Pointing, Absolute	< 0.1°
Pointing, Relative	< 0.005° Elevation < 0.03° Azimuth
Time Stamp	+/- 2 mS
Computer	PC 166 MHz
Operating System	Linux w/Ethernet connection

Table 1: Specifications of the HiRes 2 Steerable Laser System

above the horizon (see figure 6). The laser direction is "read" by rotary encoders mounted on the azimuth and zenith axes of rotation. The accuracy is listed in Table 1. The encoders are used by HR2SLS as part of a feedback loop to make small pointing corrections to ensure accurate positioning of the laser head[8].

The HR2SLS is normally run by specifying a series of shot parameters in a loop file. The loop file allows one to customize the shot geometry, filter settings, polarization, laser energies, and firing rate for an unlimited number of laser shots without changing the control program. After an operator starts the loop file, HR2SLS executes the instructions in the file until it is stopped. While the laser is running, an automatic

log is kept of the current session. All commands issued by the operator are recorded and any system warnings. The log also records the laser position, monitor probe energy, calculated energy shot into the sky, filter settings, and the time of each shot.

At the end of each night of operation, a summary is automatically created that includes: the total number of shots during the night, the number of shots per hour, total hours run, the average energy of the laser over the night, and any system warnings noted in the log files. These summary reports are posted on the World Wide Web (<http://teddy.physics.utah.edu/users/atmos/summary/>) so that the performance of the laser may be easily monitored. An example of a summary report is shown in Appendix B.

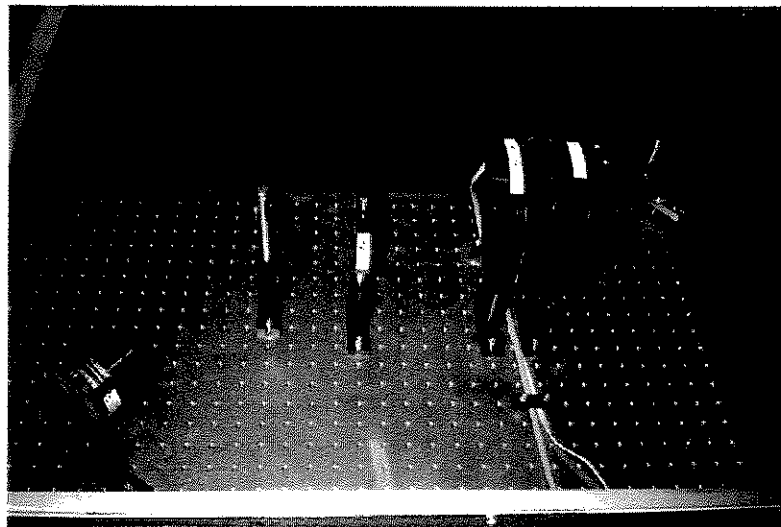


Figure 5: Photograph of the optical elements of the HR2SLS. In the foreground, one can see the monitor probe used to measure the laser energy reflected from the beam splitter. On the right are two computer controlled filter wheels that are preceded, on the left, by a $\frac{1}{4}$ -wave plate to produce circularly polarized light.

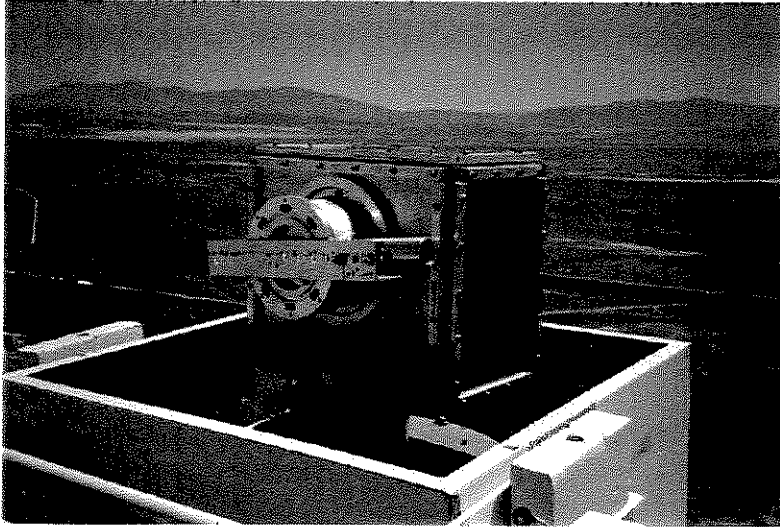


Figure 6: Photograph of the laser steering head. The HiRes detector is located on the hill in the distance directly above the near corner of the steering head.

4 THE DATA SET

The data used in this study consists of measurements made by HiRes 1 of laser shots from the HR2SLS. Once the HiRes data has been calibrated, events recorded by HiRes 1 and laser shots recorded by HR2SLS are timing-matched to separate laser events from other measurements in the HiRes 1 data stream.

Data used in this study was collected during the months of September, October, and December of 1999 and January of 2000. The data set considered contains over 100 hours of laser shots taken in various atmospheric conditions and seasons. No effort was made to remove clouds or other poor-weather measurements from the data set. The hours from each month are summarized in table 2.

Month	Hours	Comments
September 1999	60	
October 1999	18	Laser was removed for maintenance
December 1999	8	Laser was reinstalled
January 2000	20	

Table 2: Summary laser data sample.

Of the laser shots fired nightly by HR2SLS, three subsets of shots were considered for this study. These shots are pictured in figure 7.

- One set of shots sweeps out 360° in azimuth in 15° steps at 15° elevation. From this set, three symmetric pairs of shots were considered: 79° and 349° , 109° and 319° , and 124° and 304° azimuth.
- Another set covers 180° in azimuth in 15° steps at 10° elevation. From this set, the same three symmetric pairs of shots were considered.
- Another pair of shots is used that are 2° either side of the detector at an elevation angle of 0.6° . These shots pass approximately 500 meters from the detector at

their closest approach. These close shots are useful for measuring the response of the detector with minimal atmospheric effects.

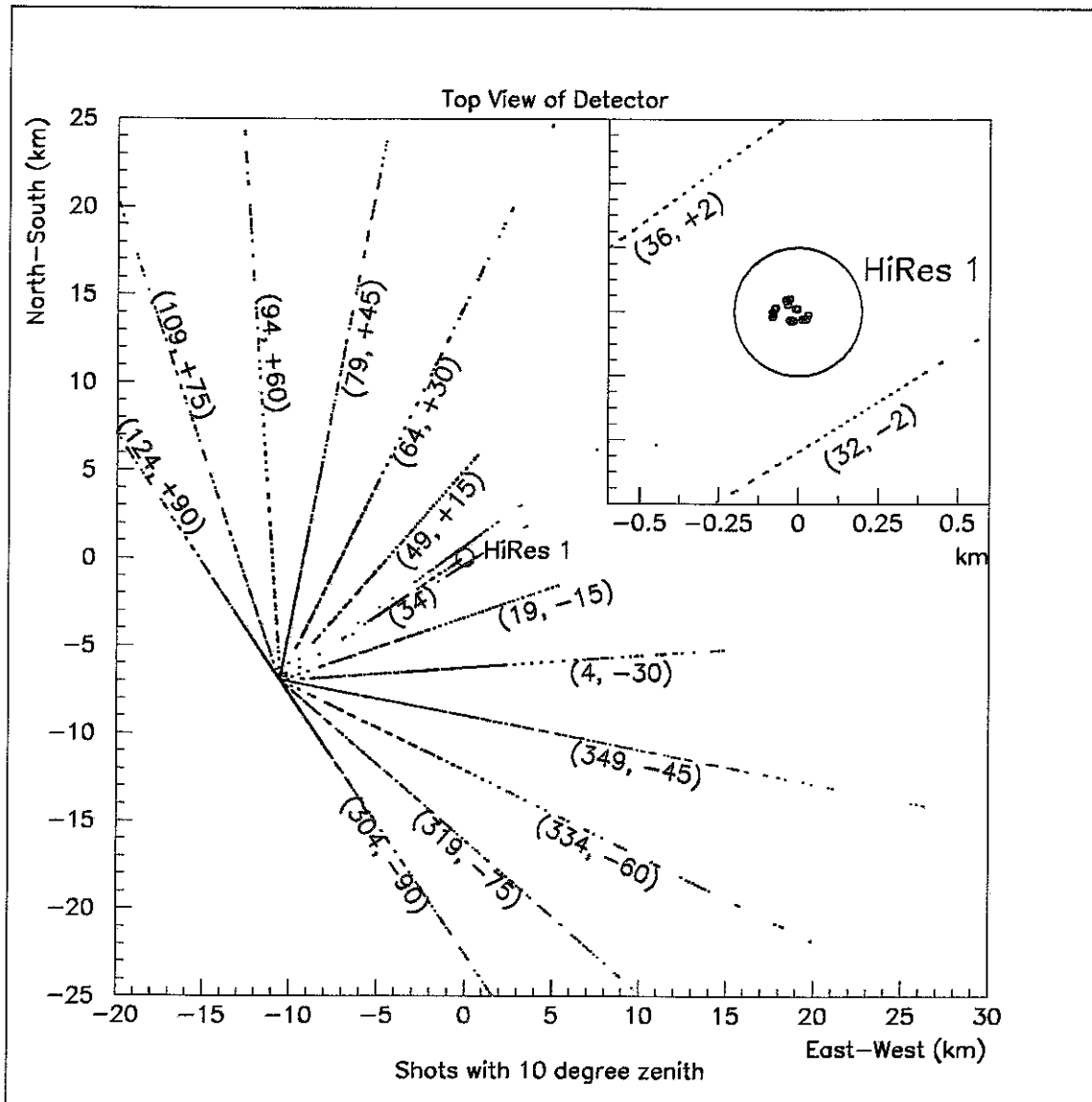


Figure 7: Laser geometries used in this study. The figure shows laser shots taken with zenith angles of 10° . Tracks in red are those tracks that were used in this study. Another set of shots, with elevation angles of 15° and the same azimuthal geometries as pictured above, were also used in this study. The inset box shows a closeup of the HiRes detector. Small circles represent mirror locations. Shots taken at a zenith angle of 0.6° and 2° either side of the detector are shown.

5 APPARATUS ASYMMETRIES

Several factors must be considered before one can attribute measured horizontal asymmetries to asymmetries in the atmosphere. The behavior of the apparatus must be well understood and be stable each night. Measured asymmetries could be attributed to any of the following effects.

- Possible Laser Asymmetries
 - Energy variation at different pointing directions.
 - Laser polarization effects.
 - Laser energy jitter.
 - Laser pointing accuracy.

- Possible Detector Asymmetries
 - Geometric effects.
 - Absolute calibration of mirrors
 - Relative calibration of mirrors

- Possible Atmospheric Asymmetries
 - Meteorological asymmetries
 - Molecular density asymmetries
 - Aerosol density asymmetries

The following explores the effect of each of these possible sources of asymmetry in the data.

5.1 POSSIBLE LASER ASYMMETRIES

5.1.1 ENERGY AS A FUNCTION OF POINTING DIRECTION

The amount of light shot into the sky by the laser varies as a function of the pointing direction of the steering head. The effect has been measured by using two radiometers and probes. One probe measures 1% of the beam inside the enclosure while a second probe measures the beam outside the laser steering head. With the energy probes in place, the laser fires several shots at positions covering the entire upper half-plane in small steps. We define the ratio,

$$R = \frac{E_{sky}}{E_{mon}} \quad (2)$$

where E_{sky} is the measurement from outside the steering head and E_{mon} is the measurement from the *monitor* probe. At each pointing direction, the ratio, R is computed. The ratios are used to create a database that records the relative brightness at each pointing direction. The energy shot into the sky is computed based on the measurement made by the monitor probe, is corrected for differences in brightness due to pointing direction, and is recorded in the data stream. The ratios in the database are an indicator of the uniformity of the laser energy over all pointing directions. When the laser was installed, every effort was made to keep the beam intensity as uniform as possible. The beam energy is not completely uniform over all pointing directions; however, the variation is small, on the order of 3% (see figure 8).

5.1.2 POLARIZATION EFFECTS

Another possible asymmetry in the laser system is variation of the polarization vector of the beam as a function of pointing direction. The polarization of the light observed by HiRes 1 has a significant impact on the measured signal. The *phase function* describes the amount of light that is scattered as a function of scattering angle. For Rayleigh or molecular scattering, the differential cross section of a scattering center is given by

$$\frac{\partial\sigma}{\partial\Omega} \propto (\sin^2(\phi)\cos^2(\theta) + \cos^2(\phi)), \quad (3)$$

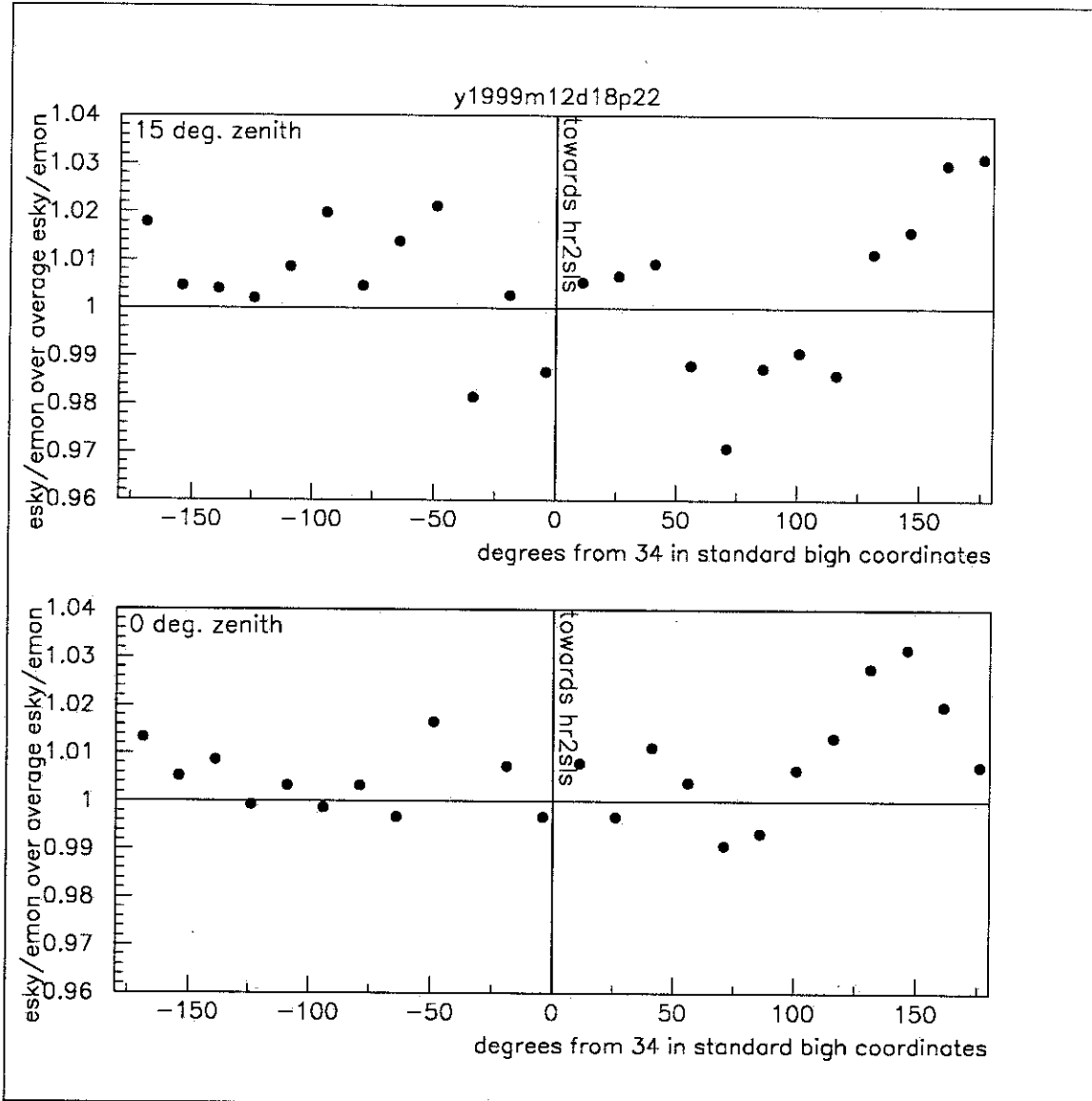


Figure 8: Light emitted from the HR2SLS as a function of pointing direction. The upper box shows the relative intensity as a function of azimuthal angle for a zenith angle of 15°. The lower box shows a similar plot for a zenith angle of 0°. The intensity never varies by more than about 3% over the entire range of azimuthal angles.

where ϕ is the angle of the light polarization (measured from a vector normal to the scattering plane) and θ is the scattering angle. Light that is vertically polarized ($\phi = 0$) exhibits no scattering angle dependence. However, with horizontally polarized light ($\phi = \pi/2$) there is a $\cos^2\theta$ dependence on scattering angle [9].

The laser produces linearly polarized light that is converted to circularly polarized light by a $\frac{1}{4}$ -wave plate. In addition to circular polarization, $\frac{1}{4}$ -wave plates in the filter wheels produce vertical and horizontal linearly polarized light when the laser is pointed towards the HiRes 1 detector at zero-degrees zenith. The filter wheels precede the mirrors that point the laser. For circularly polarized light, reflection from the steering mirrors has no effect on the polarization vector. However, for linearly polarized light, the polarization vector changes orientation upon reflection. The polarization angle is therefore dependent on the pointing direction of the steering head. For linear polarizations, the polarization vector changes symmetrically about the line between the HiRes 1 detector and the laser.

Configuring and measuring the polarization of the laser is complicated. Because polarizers for intense UV light are expensive, the beam polarization was tested by rotating an inexpensive linear polarizer sheet in front of an energy probe. The polarization vector of the HiRes 2 laser is known to about $\pm 5^\circ$.

5.1.3 LASER ENERGY JITTER

Another possible source of asymmetry is change in the laser energy as a function of time. The stability of the laser energy is listed in table 1. After a brief warmup period of approximately 15 minutes, the laser energy stabilizes¹. However, even in this stable state there is a 5% RMS shot to shot variation. The relative energy of each shot is measured and recorded in the data stream. Generally, 15 shots are fired at each location and an average energy computed to be used in data analysis.

One can imagine a situation where the average energy of the shots fired at one

¹See appendix B.

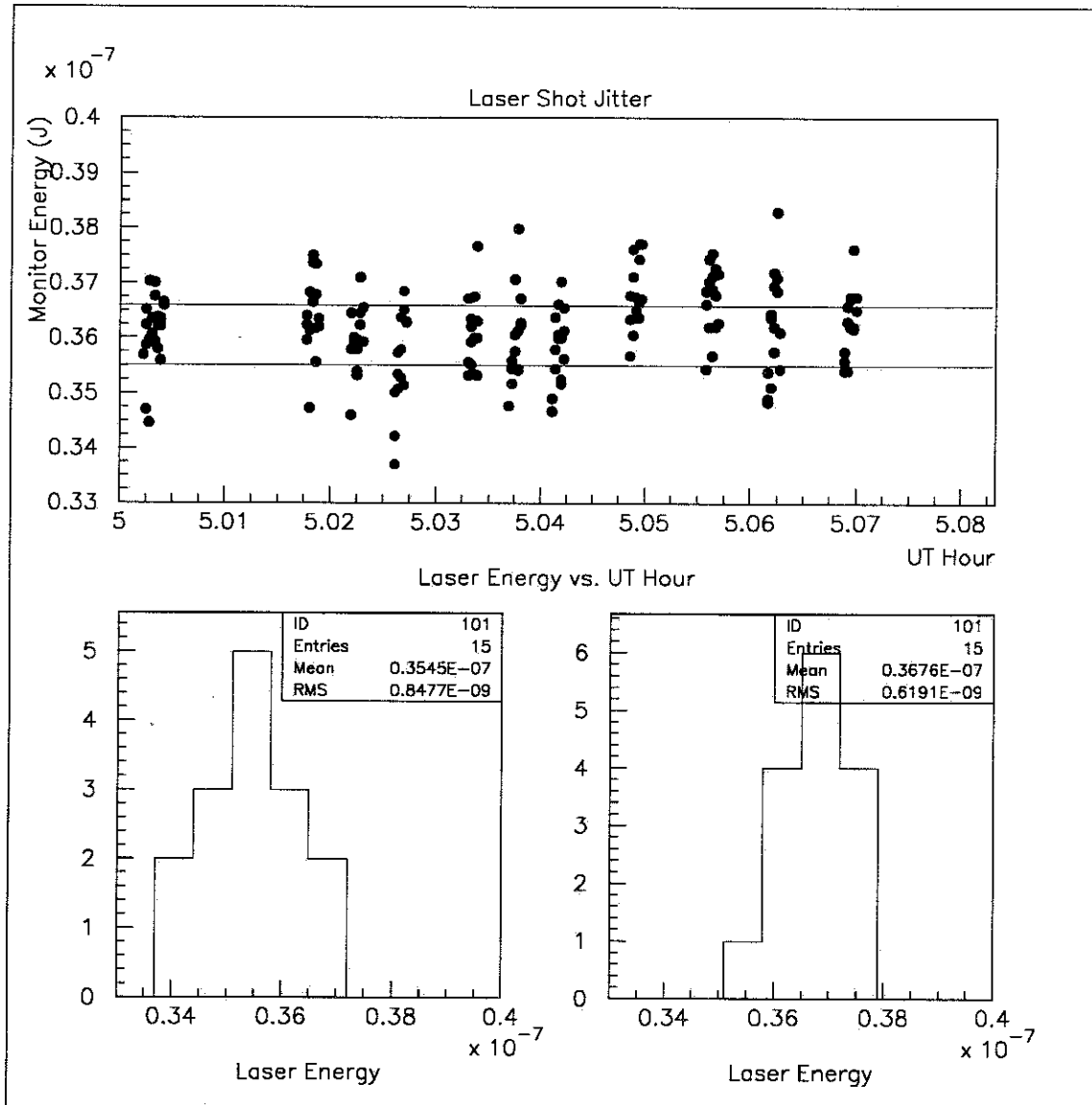


Figure 9: Comparison of laser energy from different shots over a five minute period. The top panel shows groups of shots that were taken at different laser geometries. Two of the positions are compared in the histograms below. The average laser energy for two shot geometries differs by approximately 3.5%. The analysis includes a correction for this effect.

position is higher than normal while the symmetric geometry has shots that are all abnormally low. This situation would result in the greatest error in measured asymmetry. To determine the possible error resulting from such a situation, shots from several positions were analyzed. The geometry with the greatest average energy was chosen and compared to the geometry with the smallest average energy. Figure 9 shows that random laser jitter could cause errors of around 4%.

The method used to reduce this error is to divide the number of photons observed by the HiRes 1 detector by the laser energy. As long as the relative laser energy is being measured accurately on each shot, this normalization effectively eliminates the dependence of the measured signal on the laser energy. This technique allows one to compare data from different days even if the laser energy is not entirely stable.

5.1.4 LASER POINTING ACCURACY

Another possible cause of asymmetry in the laser is the pointing accuracy of the steering head. Before the laser was installed at Dugway, laboratory tests showed the laser steering head to be accurate to within 0.1° (see table 1). At HiRes 2, pointing accuracy depends on the alignment of the laser. A target is aligned directly above the laser steering head. With the laser head positioned at 90° elevation, adjustments are made until the laser hits the vertical target. A field target located about 150 *m* away is used to verify that the laser steering head sweeps out a horizontal plane and points in the right direction. Additionally, once the laser is aligned, the HiRes 1 detector, and plane fits of the laser tracks can be used to check the laser geometry.

Perhaps most important to the study of asymmetries is that the laser pointing direction is consistent from night to night, i.e. the laser is viewed by the same PMT's every night. Slight changes in laser pointing direction can cause the laser track to cross different pixels or tubes on a mirror cluster. When the laser track is viewed by different tubes each night, light is distributed differently among the PMT's making it difficult to compare data from different nights.

One can use the track measured by HiRes 1 to extract information about the laser shot geometry. An amplitude weighted plane fit is used to compare the pointing direction of shots viewed by HiRes 1. The average vector, normal to the plane that includes the laser track and the HiRes detector, is calculated for shots at a given position. The calculated normal vectors can be compared between nights to determine the reproducibility of the laser pointing direction.

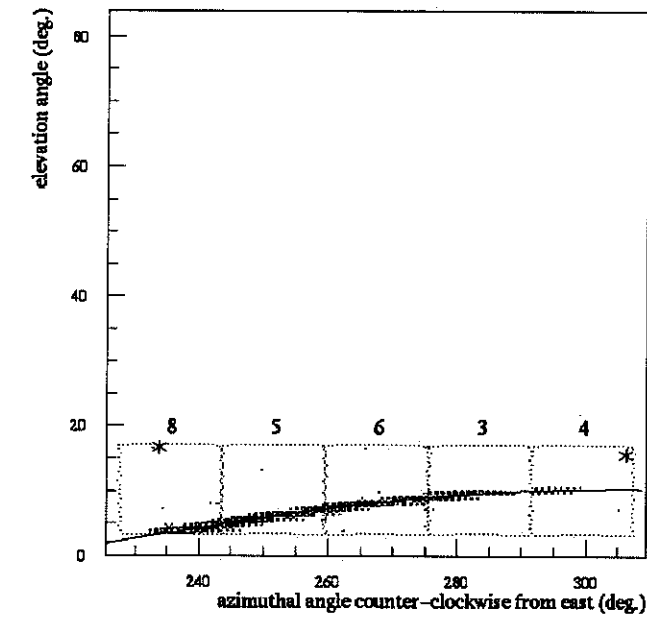
Two laser shots, one measured in September and the other in January, are pictured in figure 10. Both shots were made with the same pointing direction. The line drawn through the event represents the amplitude weighted plane that was fit to the data. The dot product between the two vectors, normal to each plane, gives the angular difference between the two laser geometries. For the two tracks pictured, the angular difference was 0.193° . The steering head is more accurate than the measured angular separation. Between the time that these two shots were taken, the laser was removed and re-installed. Differences in laser alignment could contribute to the larger than expected angular difference between the two laser shots. Moreover, this has only been a cursory study of the laser pointing accuracy and more extensive studies should be made before any conclusions are made.

5.2 POSSIBLE DETECTOR ASYMMETRIES

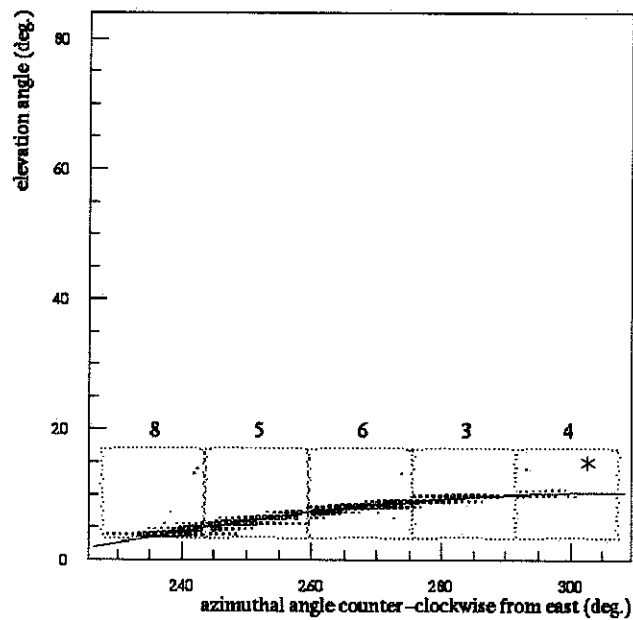
The HiRes 1 detector is composed of 5120 photo-multiplier tubes distributed among 20 mirrors. Each PMT observes a specific solid angle of the sky. A remote laser is a powerful tool for understanding the geometry of the detector and the calibration of the PMT's.

5.2.1 DETECTOR GEOMETRY

Each mirror in the HiRes 1 detector has been surveyed to determine its location and pointing direction[10]. The geometry at the HiRes 1 detector is complicated by the fact that the mirrors are on a hill and are not all at the same elevation (see



BigH 00011426 1999-SEP-04 : 18:21:14.403 165 697



BigH 00011551 2000-JAN-07 : 18:27:27.245 480 951

Figure 10: Laser shots taken at 319° azimuth and 10° elevation. The top laser shot was taken in September, 1999 while the lower was taken in January of 2000. According to an amplitude weighted plane fit, the pointing direction of the two tracks differs by approximately 0.193° .

table 2). When the detector measures nearby laser shots, parallax, caused by the separation between mirrors and differences in mirror height, produces discontinuities at mirror boundaries. This effect is pronounced with laser shots because the beam passes through the field of view of several adjacent mirrors. Distant laser tracks or downward going cosmic ray events are far enough away that any separation between mirrors is negligible.

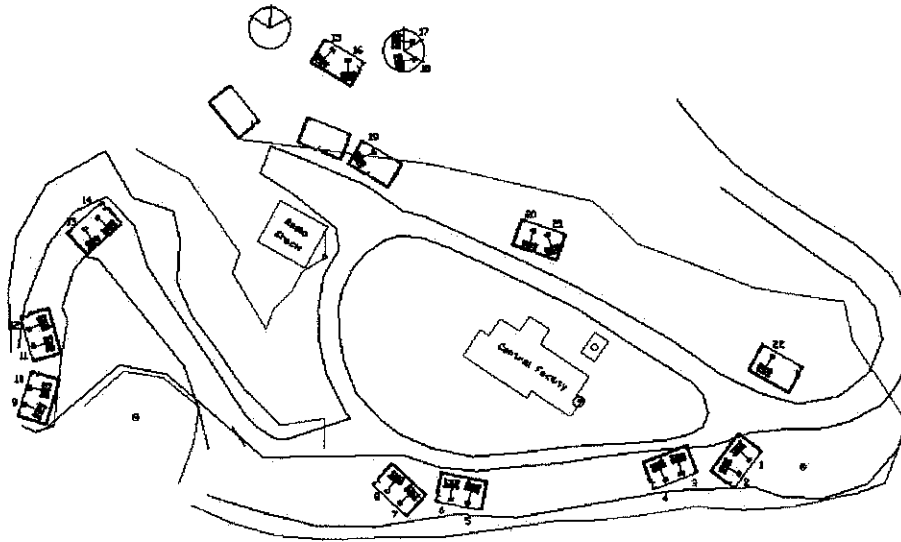


Figure 11: A map of the HiRes detector.

5.2.2 ABSOLUTE CALIBRATION

Detector calibration is also important. This problem can be separated into two parts. First, it is important to get an accurate *relative calibration*; A given light source should yield the same response when measured by different mirrors. Second, it is important to understand the *absolute calibration* so that an accurate photon flux can

Mirror Number	x-coordinate	y-coordinate	z-coordinate
1	24.78	-20.77	-3.23
2	23.04	-23.26	-3.23
3	15.58	-22.08	-2.98
4	12.76	-23.15	-2.98
5	-16.13	-26.70	-3.35
6	-19.09	-26.08	-3.35
7	-25.11	-27.74	-3.34
8	-27.38	-25.57	-3.34
9	-81.82	-15.10	-6.31
10	-80.91	-12.25	-6.31
11	-80.70	-4.44	-6.35
12	-81.56	-1.63	-6.35
13	-74.11	11.03	-5.24
14	-71.77	13.22	-5.24
15	-39.42	38.49	-4.33
16	-35.26	36.17	-4.33
18	-27.05	41.39	-3.05
19	-33.58	23.14	-1.08
20	-7.76	10.61	-2.89
21	-4.15	9.61	-2.89
22	29.25	-9.07	-4.24

Table 3: The relative position of each mirror in the HiRes 1 detector. All measures are in meters

be calculated from the measured detector signal. For the purposes of this study, the relative calibration is the most important.

One method of absolute calibration uses a roving xenon flasher. The flasher emits pulses of UV light. Nearly the same number of photons are emitted at each flash. The shot to shot RMS is better than 7%. External, neutral-density filters are mounted on the flasher to produce different intensities. The flasher is used to “expose” the PMT cluster of each mirror to various intensities of light and measure its response[11]. Poisson statistics are used to find gains for each PMT and non-linearities in each tube are treated. This “new” calibration method is still under development.

Laser shots that pass close to the detector are useful for calibration comparisons because they are viewed by several mirrors, and for scattering angles greater than about 20° , are less sensitive to atmospheric effects. One can compare the amount of light seen in the data to Monte Carlo simulations that predict what the detector *should* see in an idealized atmosphere. Simulating laser events is a powerful tool for understanding the effects of different laser geometries, energies, atmospheric conditions and detector responses. In figure 12, Monte Carlo predictions for various atmospheric conditions are shown. In this case, the mixing layer and scale height have been kept constant and only the extinction length was changed.

Using the laser data, calibrated with both the old and new methods, one can compare the differences between calibrations. From the preliminary results, it appears that the new calibration yields approximately 25% less photons than the old calibration. Neither method agrees well with Monte Carlo predictions. Figure 13 shows a comparison of both the old and new calibrations to a Monte Carlo prediction. It appears that there is still some work to be done before the absolute calibration of the HiRes detector is well understood.

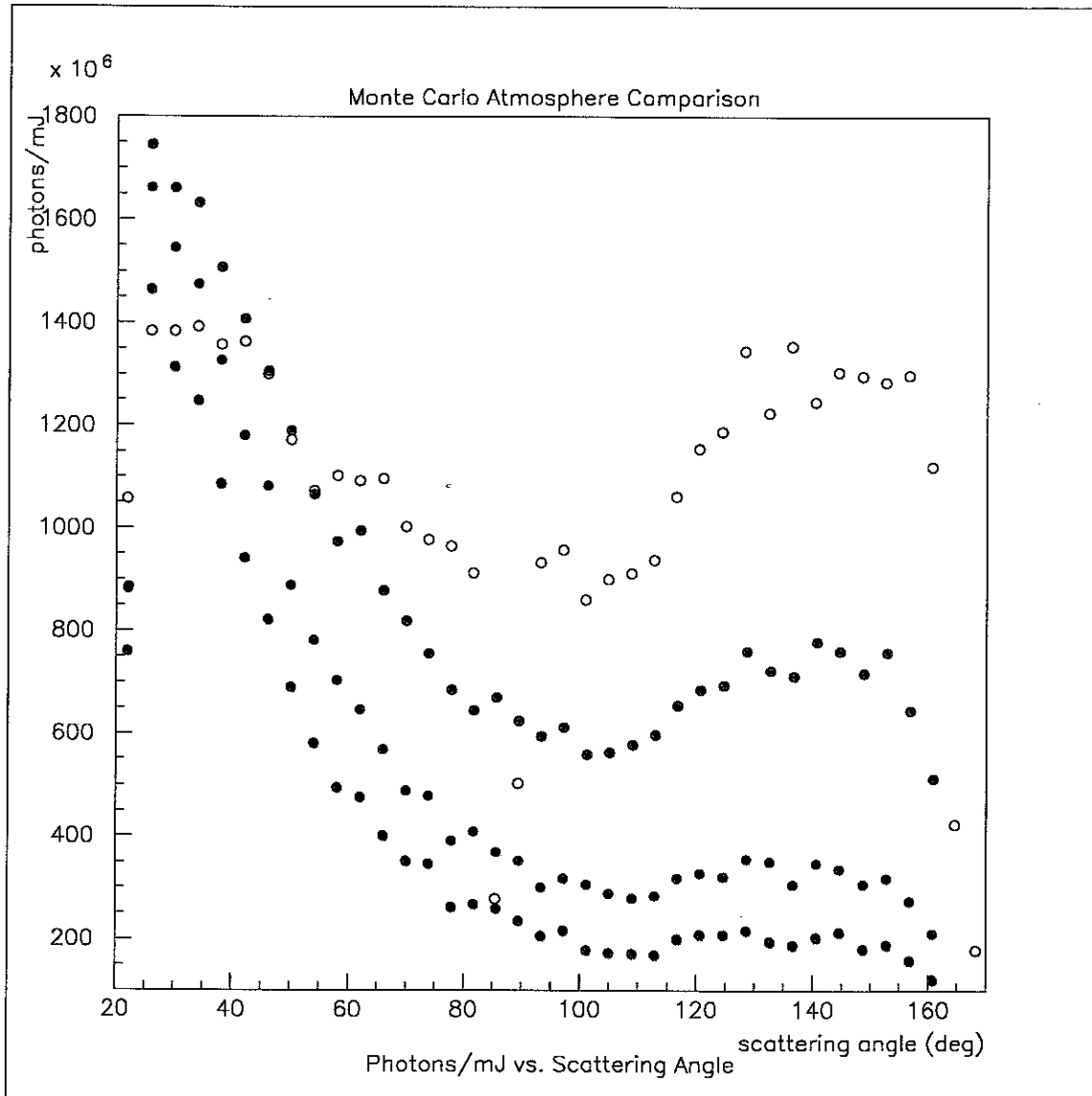


Figure 12: Profiles of Monte Carlo simulated laser shots, with a geometry of 36° azimuth and 0.6° zenith, in four different atmospheres. The open circles are for a molecular atmosphere. Atmospheres with aerosol extinction lengths of 25 km , 9 km , and 6.5 km are shown by black, red, and blue markers respectively.

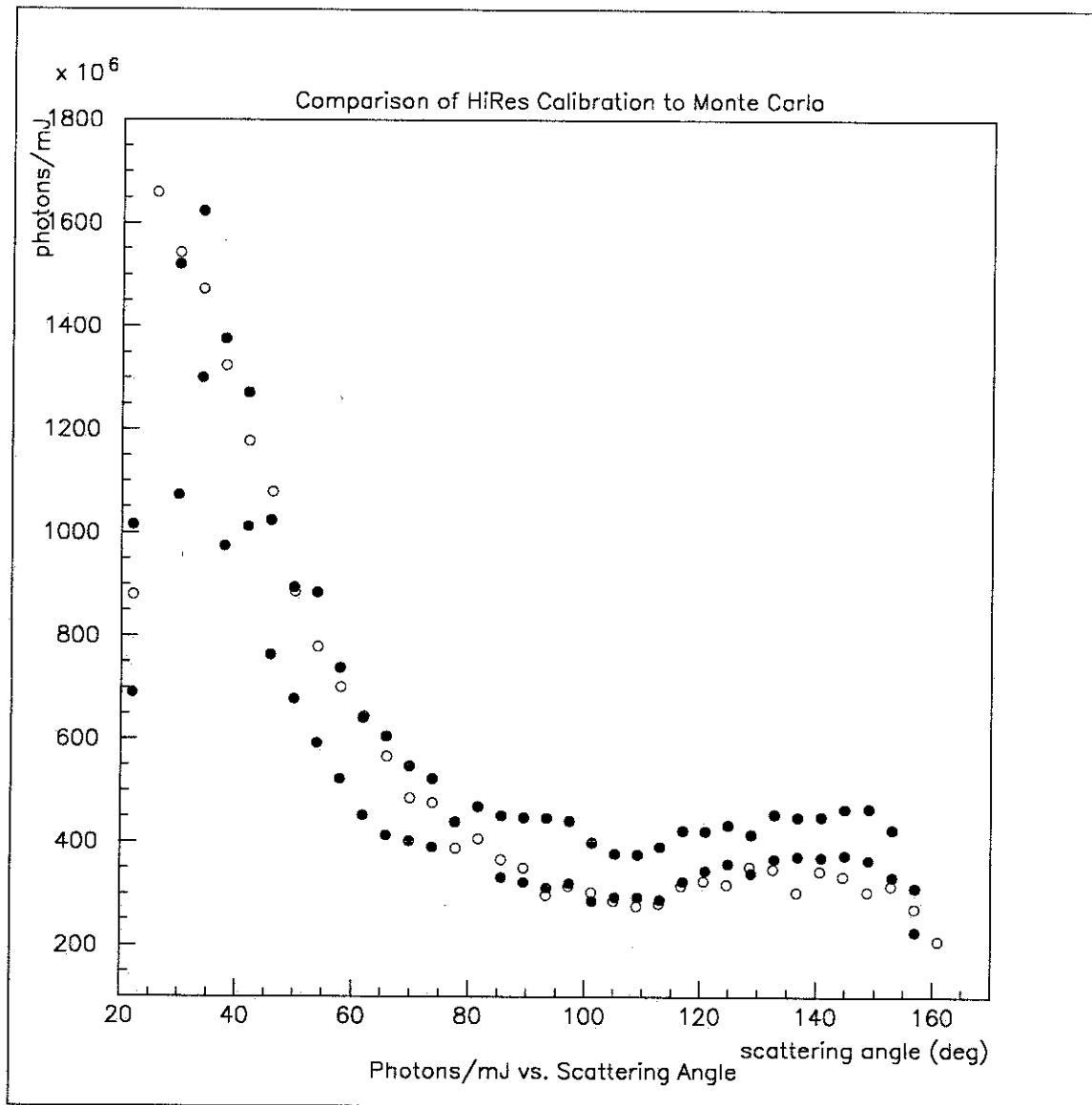


Figure 13: A comparison of data calibrated using both the old and new methods, shown by black and blue markers respectively, for a laser shot at 0.6° zenith and 36° azimuth. A Monte Carlo prediction for an aerosol extinction length of 9.0 km is superimposed in red.

5.2.3 RELATIVE CALIBRATION

Although the absolute calibration of the HiRes 1 detector is a crucial part of accurately reconstructing cosmic ray events, it is not particularly crucial to the study of horizontal symmetry in the atmosphere. One method that can be used to monitor the symmetry of the atmosphere is to compare the amount of light measured from symmetric laser tracks to light, measured from the same tracks, on another day. Mathematically the idea can be represented by the following.

Consider a function $L_N(x)$ that describes the amount of light scattered from the laser beam as a function of distance, x . Here, $L_N(x)$ describes a laser shot on the North side of the detector. A similar function, $L_S(x)$ can be defined for the symmetric laser geometry on the South side of the detector. The measured HiRes signal is represented by

$$C_N L_N(x)$$

where C_N is a function that describes the response of the calibrated HiRes 1 detector. Similarly, for the South track, we have

$$C_S L_S(x).$$

Next, we define the ratio,

$$R = \frac{C_N L_N(x)}{C_S L_S(x)} \quad (4)$$

to describe the amount of light that we see on one side of the detector compared to the other side. However, we still have the constants, C_N and C_S that bias our measurement of the atmosphere with unknown detector effects. To work around this problem, we define a second ratio

$$\tilde{R} = \frac{\tilde{C}_N \tilde{L}_N(x)}{\tilde{C}_S \tilde{L}_S(x)} \quad (5)$$

where \tilde{R} is the same as the ratio above but for a *reference day*. The reference day is used to divide out detector effects so that atmospheric effects alone can be studied. If we assume that the constants, C_N and C_S do not depend on time, i.e. that the response of the HiRes 1 detector does not change significantly from night to night,

then

$$C_N = \tilde{C}_N$$

and

$$C_S = \tilde{C}_S.$$

Which allows us to take the ratio of the two ratios, R and \tilde{R} , to obtain

$$\mathcal{R} = \frac{R}{\tilde{R}} = \frac{\frac{C_N L_N(x)}{C_S L_S(x)}}{\frac{C_S \tilde{L}_S(x)}{C_N \tilde{L}_N(x)}} = \frac{\frac{L_N(x)}{L_S(x)}}{\frac{\tilde{L}_N(x)}{\tilde{L}_S(x)}} = \frac{L_N}{\tilde{L}_N} \frac{\tilde{L}_S}{L_S}. \quad (6)$$

Notice that equation 6 is independent of C_N and C_S , meaning that \mathcal{R} is independent of the absolute calibration of the HiRes detector. As long as the response of the HiRes detector is not different for the *test day* (R) and the *reference day* (\tilde{R}), then equation 6 is valid.

6 **ATMOSPHERIC ASYMMETRIES**

Possible sources of asymmetry in the atmosphere are uneven molecular distributions, meteorological effects (such as clouds and precipitation), and uneven aerosol distributions. A brief description of each follows.

6.1 **MOLECULAR ASYMMETRIES**

We expect the variations in the molecular part of the atmosphere to be small. The distribution of molecules in the atmosphere is almost strictly a function of elevation and relatively independent of geography. Measurements have shown that a simple, pressure dependent model adequately describes the distribution of molecules in the atmosphere even at large distances[12][13]. Variations in the molecular part of the atmosphere are caused by changes in air pressure. Variations from the average molecular density are small (on the order of $\sim 3\%$ of the average density) and can be ignored[14].

6.2 **METEOROLOGICAL ASYMMETRIES**

Meteorological asymmetries are typically caused by clouds, precipitation, and strong wind. From common experience, we know that clouds and precipitation are not uniform. Although meteorological effects are generally detrimental to measuring light from cosmic rays and laser shots, they do provide an obvious means for testing the effectiveness of a method for identifying atmospheric asymmetries.

The effects of clouds on a laser shot are huge compared to other light scatterers. Clouds are more optically dense than most other aerosols and absorb a great deal of infrared radiation. For optical and shorter wavelengths, clouds are very efficient scatterers of radiation. Light scattering from a single cloud droplet scatters preferentially in the forward direction. However, because of the huge number of scattering centers, multiple scatters diffuse a laser beam, incident on a cloud, almost completely.

The ratio method described in section 5.2.3 can be used to look for the asymmetric effect of clouds in the data. Figure 14 shows data from a laser shot that has been partially obscured by a cloud. A short description of each of the six panels in figure 14 follows.

6.3 \mathcal{R} -PLOTS

This section describes the ratio plots (\mathcal{R} -plots) proposed in section 5.2.3 and how they are used to study atmospheric asymmetries. Figure 14 will serve as an example for illustrating the \mathcal{R} -plot method. In the figure, the laser pointing directions are 109° azimuth for the North track and 319° azimuth for the South track. Both shots use an elevation angle of 10° .

A profile of the North laser track is shown in the upper left panel. The number of photons per mili-joule of laser energy are plotted on the y-axis versus the total distance that the laser light has traveled. Different mirrors are plotted with different color markers to help identify boundaries between mirrors.

On the upper right panel, the photons measured in the North track are divided by the number of photons measured on a reference day. The nominal line, $y = 1$ is plotted. Points above the $y = 1$ line are brighter than the reference day while those below are dimmer. The second row of panels are the same as those above only they are made for the Southern shot, symmetric to that above.

The bottom left panel shows the photons in the North track divided by the photons in the South as a function of total path length. Points above the $y = 1$ line indicate more photons measured in the North track than in the South track. This ratio is described in equation 4 and contains detector calibration effects. The bottom right panel is the ratio described in equation 6 which we will call an \mathcal{R} -plot. The ratio shown in the upper right panel is divided by that of the middle right panel. This ratio of two ratios is independent of the absolute calibration of the HiRes detector. Points above the $y = 1$ line indicate that ratio, $\frac{L_N(x)}{L_S(x)}$ is larger than the same ratio

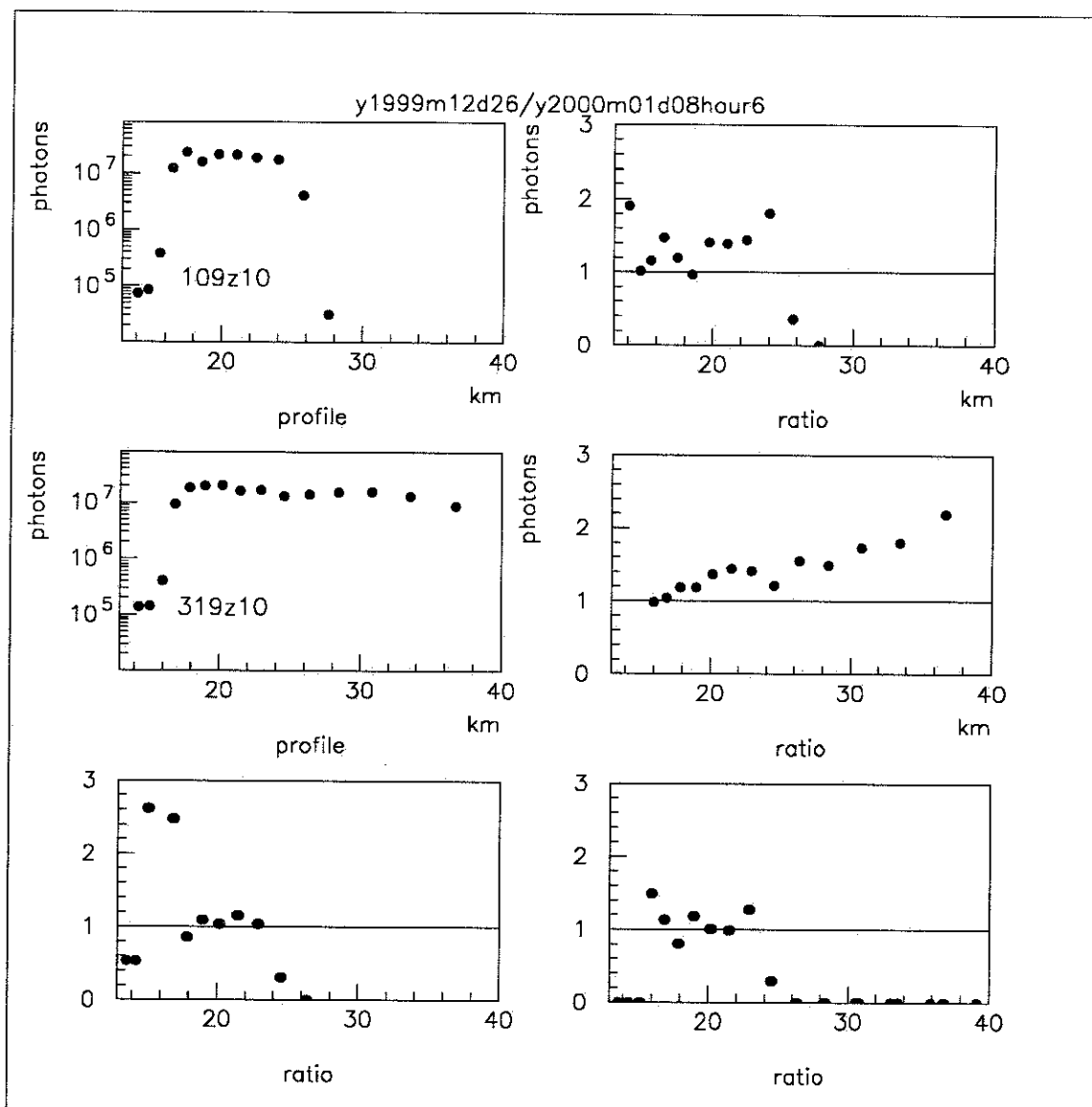


Figure 14: Plot of ratios for data taken on the 8th of January, 2000. Notice the deviation from one in the \mathcal{R} -plot (bottom right panel) indicating that more light was measured on the South side of the detector than on the North.

for the reference day. That is, more light is observed on the North than on the South than was measured for the reference day. Points on or near $y = 1$ indicate that the atmosphere is generally uniform. The greater the distance from one; the greater the measured asymmetry.

The \mathcal{R} -plot (the lower right panel) shown in figure 14 depicts a large asymmetry beginning around 20 km. In this case, the North track passes behind a cloud and is obscured from the detector. No photons are measured in the North after it passes behind the cloud. Event displays for both the North and the South geometries are shown in figure 15.

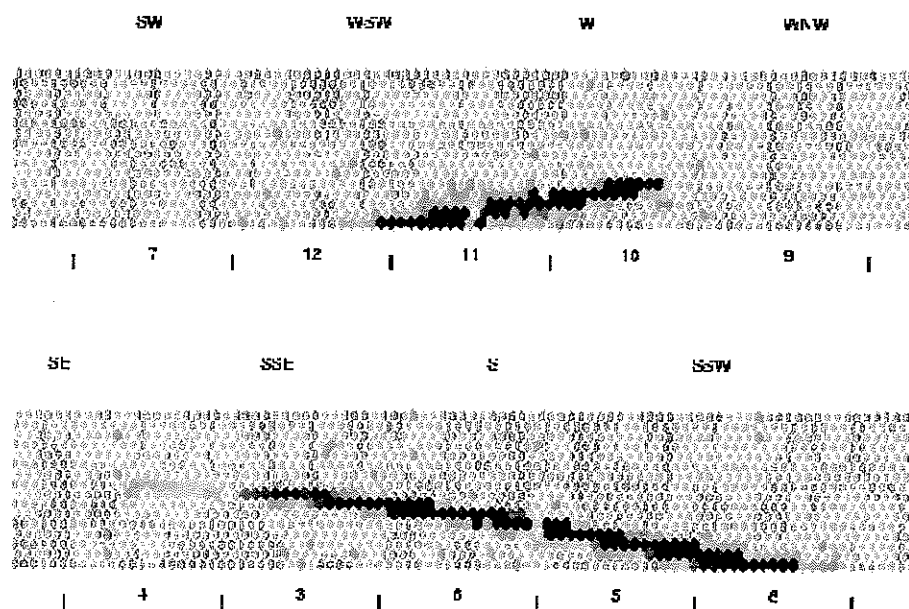


Figure 15: The top panel shows the North track (azimuth=109°) being obscured by a cloud. The bottom panel shows the symmetric track on the South side of the detector (azimuth=319°). This track was not impeded by cloud cover and is detected by several more mirrors. Both laser shots were taken during the same hour and have the same zenith angle of 10°.

From figure 14, it appears that we are able to identify large atmospheric asymmetries using the \mathcal{R} -plot method. Asymmetries caused by inhomogeneous distributions of aerosols are sure to be much smaller than asymmetries due to clouds. Does this

same technique work to identify asymmetries more subtle than those caused by clouds?

6.4 AEROSOL ASYMMETRIES

Changes in the aerosol extinction length are observed in the laser data collected by HiRes 1. In the presence of large concentrations of aerosols, light scatters preferentially at small scattering angles according to the aerosol phase function. Therefore, in dense aerosols, profiles of laser shots appear to be brighter at small scattering angles than at large scattering angles. Moreover, dense aerosols produce extinction lengths that are much shorter than those for a molecular atmosphere. Light scatters from tracks in dense aerosols more efficiently. For scattering angles greater than about 40° , laser tracks in dense aerosols appear dimmer than shots measured in a molecular atmosphere.

An example of an atmosphere with a high concentration of aerosols is shown in figure 16. The shots pictured were collected on September 7, 1999. These shots pass very near the detector and only span about 1 *km* of atmosphere. The two upper right panels show the ratio of the measured signal to a reference day. At small scattering angles, there much more light than was observed on the reference day. However, as the scattering angle increases, the amount of light drops dramatically until there is only about half as much light measured compared to the reference day. This shape in the ratio plots is indicative of a high concentration of aerosols. The \mathcal{R} -plot (lower right panel) shows that the atmosphere looks uniform, which is to be expected for measurements on small distance scales.

Laser geometries that probe the aperture of the HiRes detector further show atmospheric asymmetry. Figure 17 shows laser shots taken 45° either side of the detector (azimuth angles of 79° and 349°)². The \mathcal{R} -plot shows that the number of photons observed on the North versus the South sides of the detector is significantly

²see figure 7 for picture of geometry of the laser shots and the HiRes detector

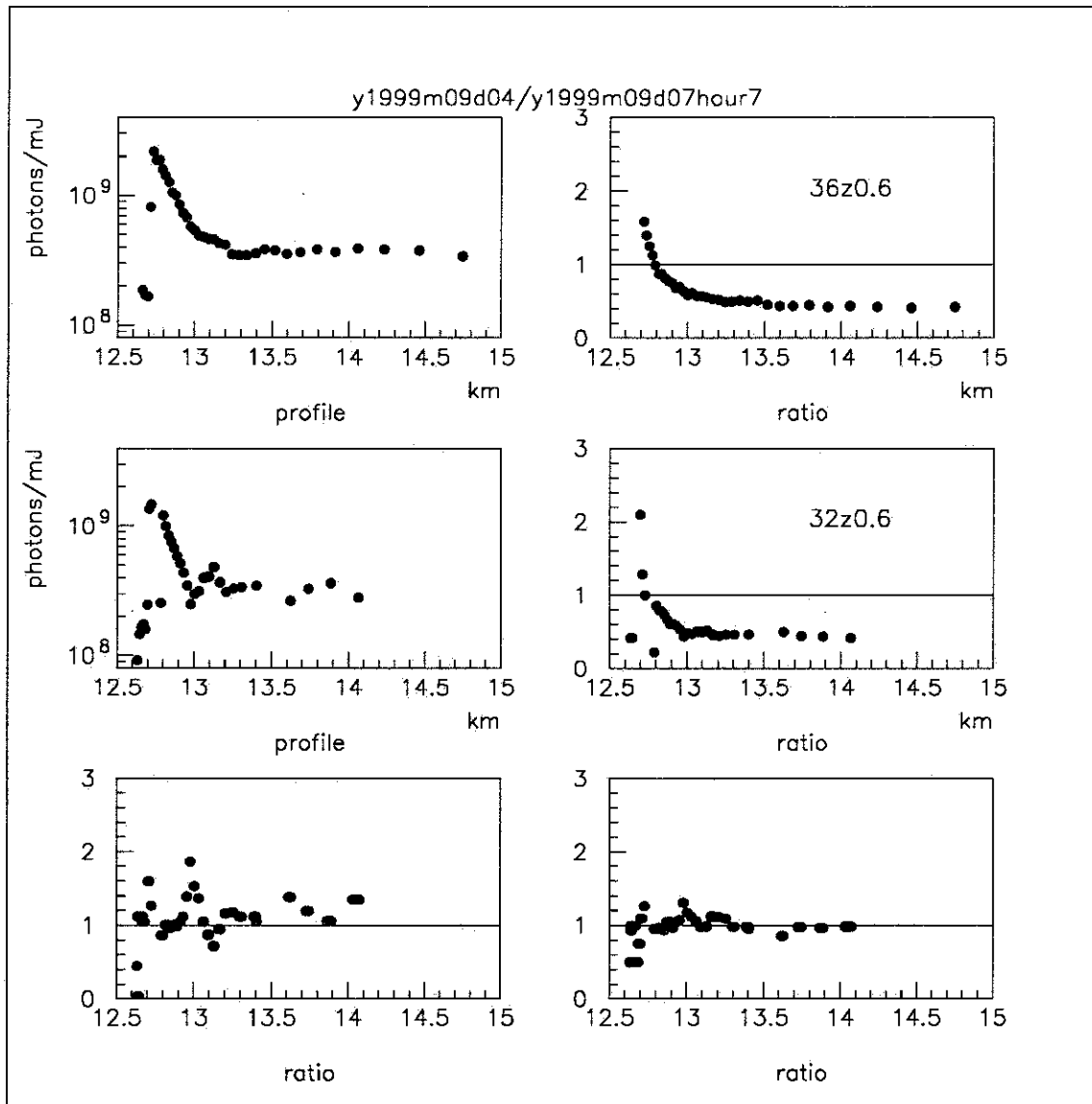


Figure 16: Data taken on September 7, 1999. The atmosphere has a high concentration of aerosols shown by the sharp peak in the upper two right panels. The laser shots shown pass very near the detector (azimuth angles of 36° and 32° at 0.6° elevation). At small distances, the atmosphere appears to be uniform.

larger (approximately 50% more) than was observed on the reference day. There is a “hole” in the profile for the shot at 349° because one of the mirrors of the detector was not running when this data was taken. Unfortunately, the missing mirror views most of the shots that probe the detector’s aperture further. With the mirror missing, a significant portion of more distant laser tracks is missing making it difficult to measure other possible asymmetries.

Animations of the \mathcal{R} -plots, taken during a given month, have become a useful tool for monitoring atmospheric asymmetries. Animations provide a convenient means for identifying asymmetries and for tracking their time evolution. Because it is impossible to include any animations in this paper, several “frames” are included in appendix A illustrating the time evolution of the asymmetry measured on September 7, 1999. In addition, \mathcal{R} -plots from each hour that data was taken on September 7, 1999 are pictured in figure 18. \mathcal{R} -plots from laser shots taken at azimuth angles of 79° and 109° azimuth are pictured. During these four hours of data, the time evolution of the asymmetry is observed. Most of the change in the asymmetry occurs in the North laser track. Laser profiles for both the North and South tracks are shown in appendix A.

Data from September 9, 1999 (two days later), shows no sign of the asymmetry measured on September 7 and shown in figure 17. The \mathcal{R} -plot for the 9th shows that the light on either side of the detector is similar to that measured on the reference day (see figure 19). By September 9, the atmosphere at HiRes had cleared significantly and the source of the measured atmospheric asymmetry on the seventh had disappeared.

The aerosol content on the seventh was extremely high. Monte Carlo simulations were run using several different aerosol extinction lengths to duplicate the asymmetry measured on September 7. The same analysis used on the real data was applied to the Monte Carlo data using one extinction length for the North track and different extinction length for the South track. One combination that produced an asymmetry similar to that measured on the seventh was an extinction length of 12 *km* for the

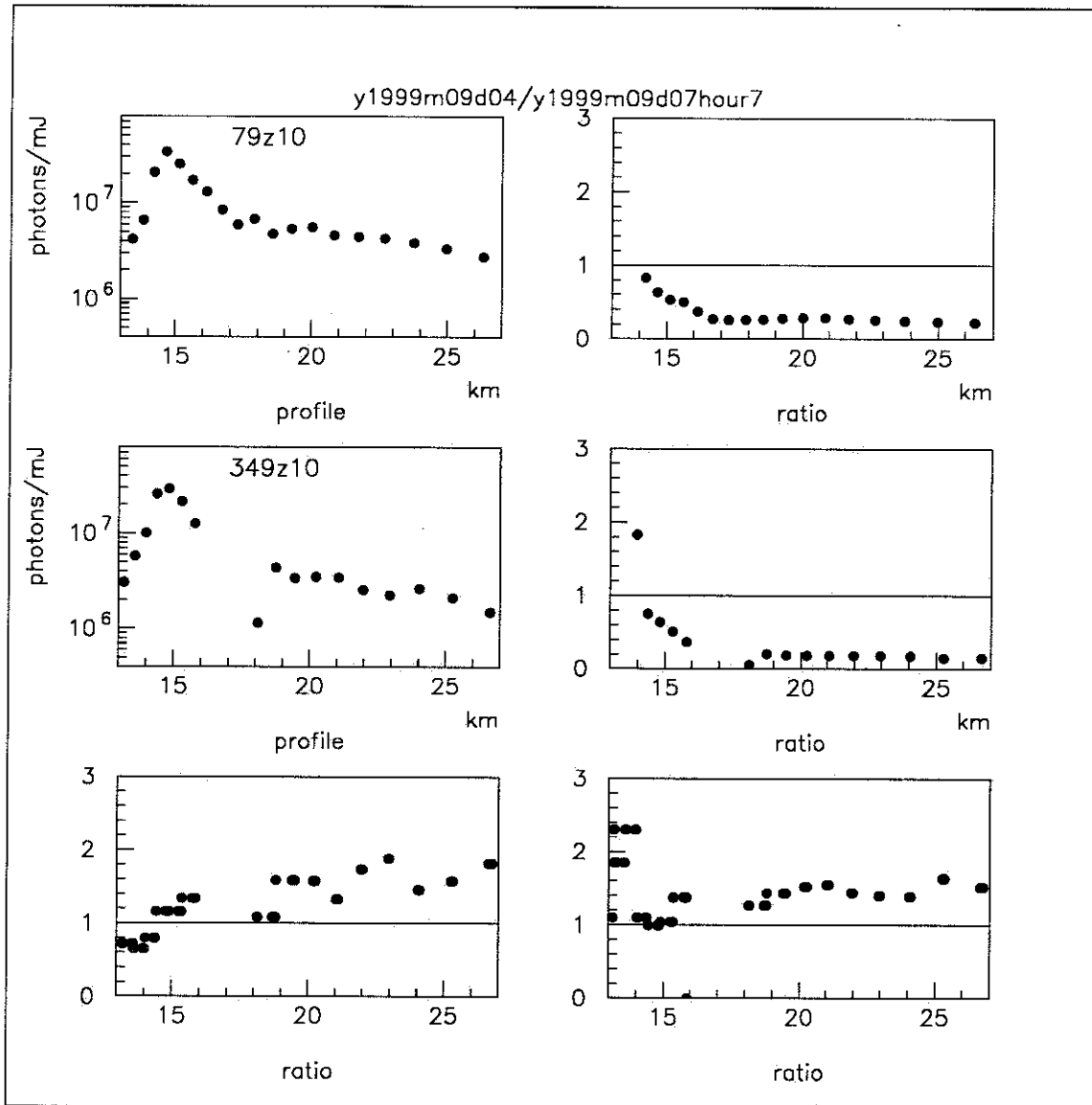


Figure 17: Data taken on September 7, 1999. Azimuth angles of 79° and 349° are shown. Both shots have elevation angles of 10° . The atmosphere has a high concentration of aerosols. There is a “hole” in the track at 349° because a mirror of the HiRes detector was not run this evening. The \mathcal{R} -plot shows that there is a large atmospheric asymmetry measured between the two sides of the detector. In this case, the Southern track is significantly dimmer than the Northern track.

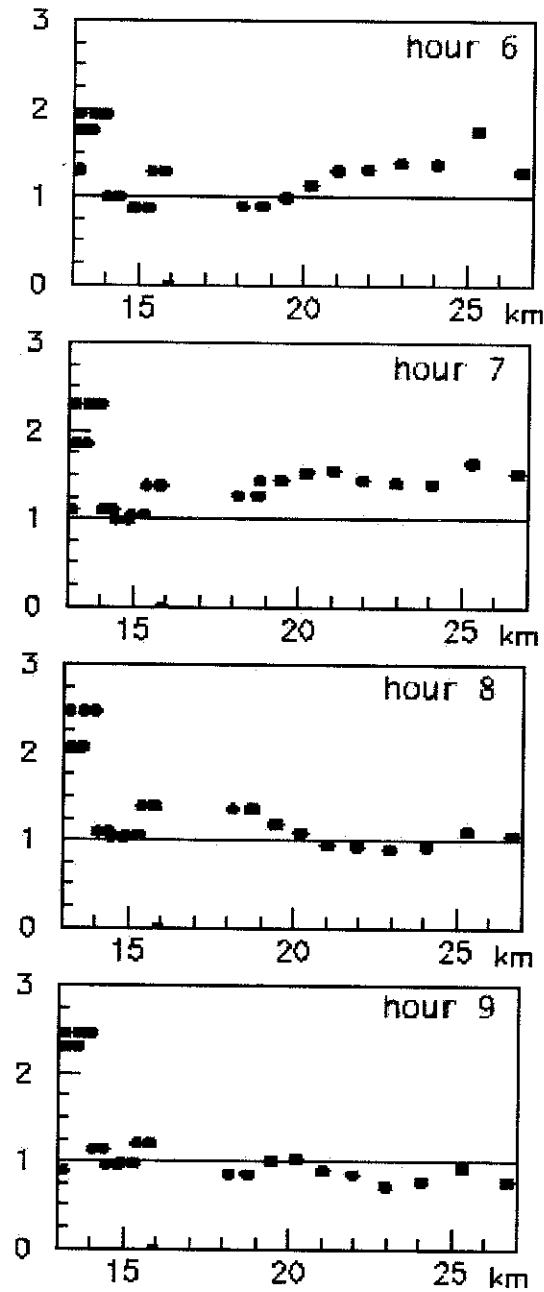


Figure 18: Each row shows \mathcal{R} -plots from a given hour. The laser geometry shown is 79° and 349° azimuth and 10° zenith. Beginning in UT hour 6, the asymmetry is measured at distances greater than 20 km . By hour 7, the asymmetry has moved closer and is now observed at distances greater than 18 km . In UT hour 8, the asymmetry is observed at distances that are less than 20 km . The asymmetry continues to move until it has mostly passed by hour 9. Laser profiles, shown in appendix A, demonstrate that most of the measured asymmetry comes from changes in the North track.

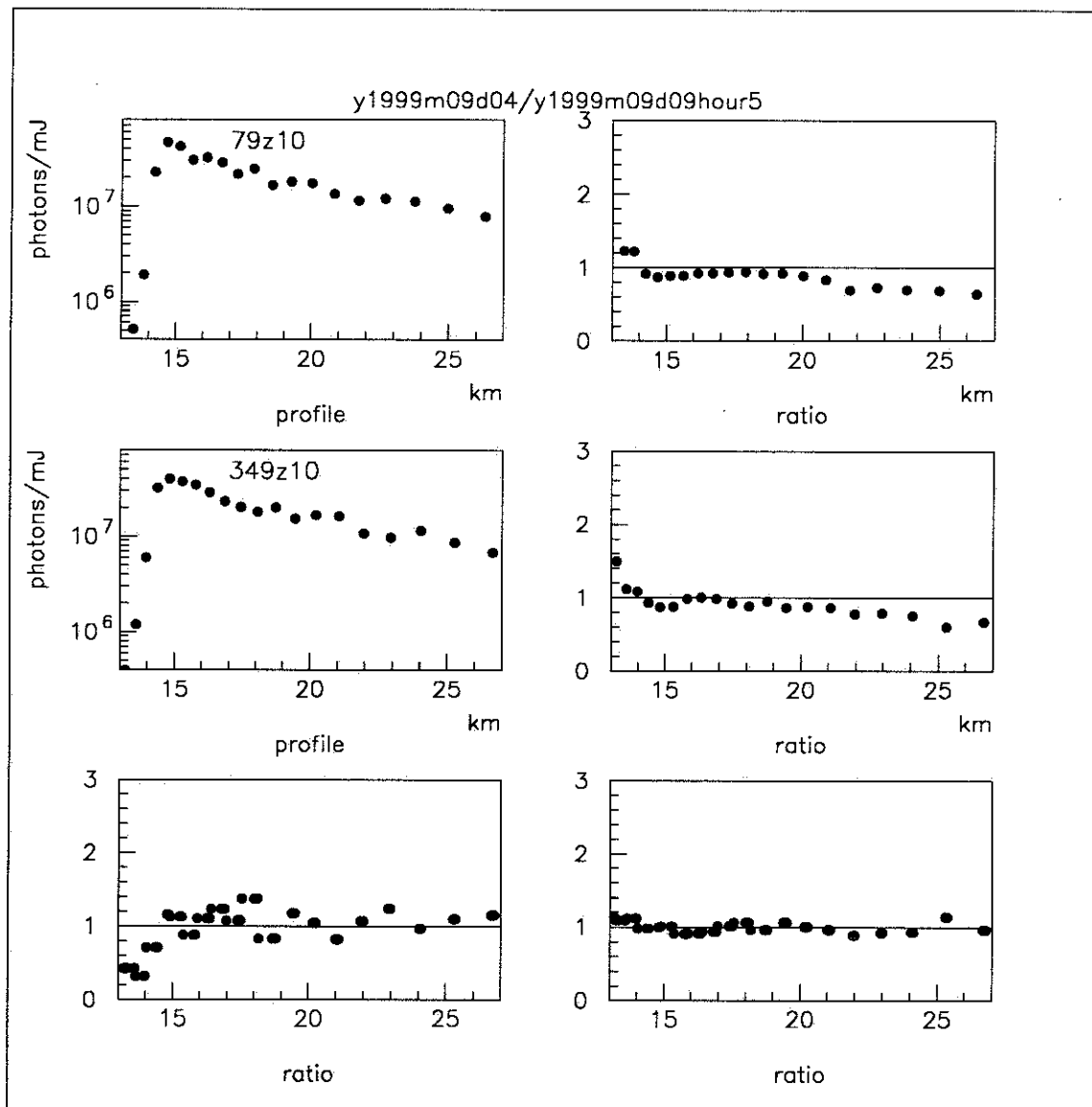


Figure 19: Data taken on September 9, 1999. The atmosphere has a much lower aerosol concentration compared to September 7. The asymmetry measured on September 7, 1999 (figure 17) is gone. The number of photons measured on either side of the detector, now agree with the measurements made on the reference day. The optical clarity of the atmosphere is symmetric.

North track and 9 *km* for the South (see figure 20). Several different combinations of extinction lengths could produce asymmetries similar to that shown. However, it appears that the asymmetry measured on the seventh of September is consistent with an extinction length difference of about 3 *km* between the two sides of the detector.

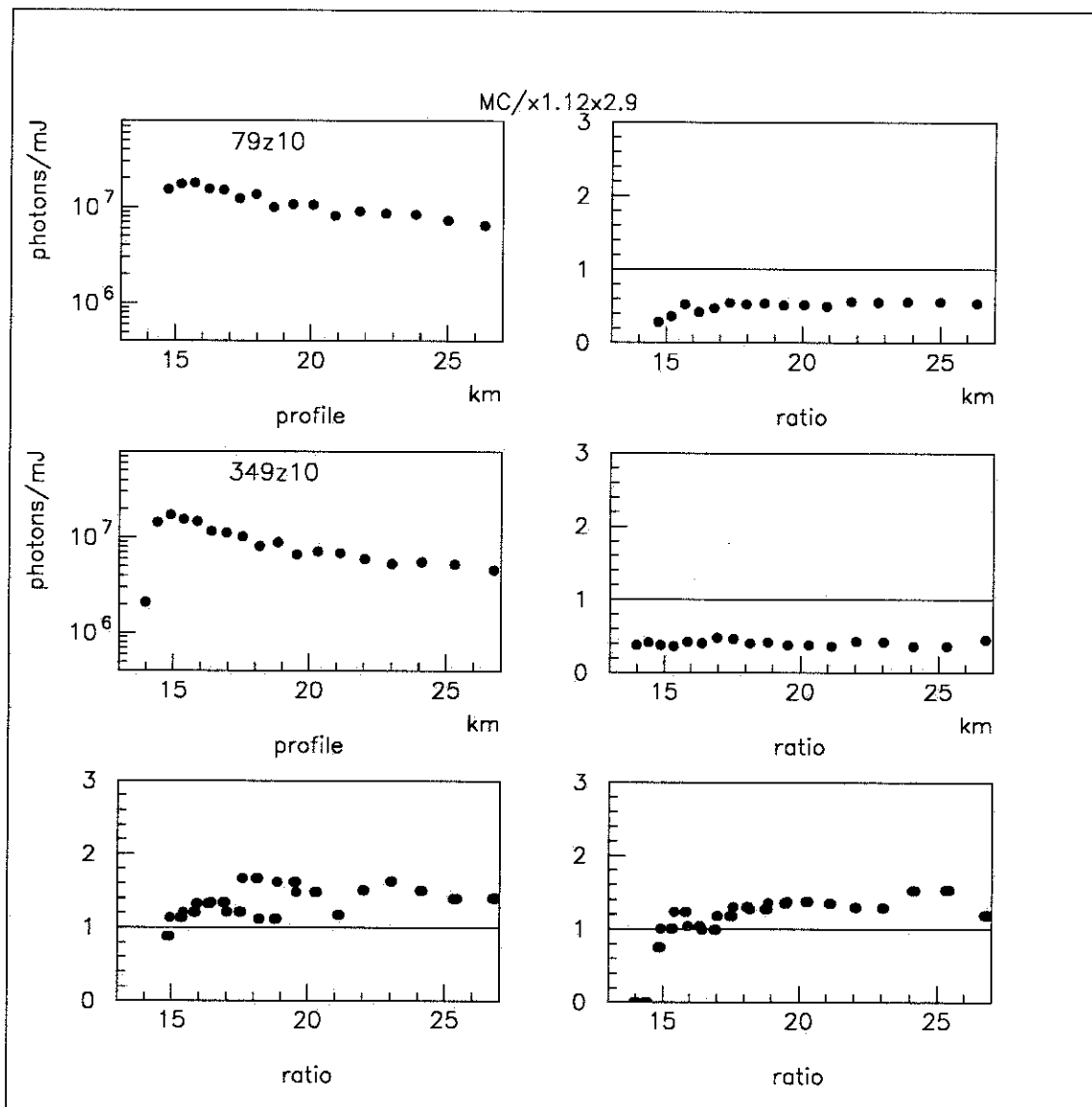


Figure 20: Monte Carlo data generated to replicate the asymmetry measured on September 7, 1999. The North track was generated using an aerosol extinction length of 12 km while the South was generated with 9 km. The extinction length difference produces an asymmetry that appears to be consistent with that measured on September 7, 1999.

6.5 TRENDS IN ASYMMETRY

We have shown that we are able to measure atmospheric asymmetries at HiRes. Not only are we able to measure spatial asymmetries but we are also able to monitor their time evolution. Asymmetries could be caused by dust storms or incoming fronts. If measured asymmetries are random, over large periods of time, we would expect them to average. At times, more light would be measured on the North than the South and at other times, more light on the South than the North. However, trends in the asymmetries, on large time scales could suggest a geography dependent aerosol distribution.

In order to generalize the data taken over the four months of this study, histograms were created from the data shown in the \mathcal{R} -plots. Data points, from over 400 \mathcal{R} -plots, were collapsed onto the y-axis and plotted as a histogram. Data from a unique geometry and month are plotted on the same histogram. A uniform atmosphere would produce a distribution with a mean of 1 with a very small standard deviation. However, if the atmosphere was consistently asymmetric during the month, one would expect a mean that was offset from 1 by a distance proportional to the magnitude of the asymmetry. Histograms with large standard deviations and means close to 1, suggest a randomly asymmetric atmosphere. Each month is plotted separately to identify possible seasonal changes in aerosol distributions. Figures 21 through 28 show the histograms obtained from the \mathcal{R} -plots.

The histograms suggest that the atmosphere is generally symmetric at small scales. Shots that span larger area are more sensitive to asymmetries. The standard deviation for shots that are far from the detector are generally greater than shots that are nearby. It is difficult however, to identify any systematic asymmetry at HiRes from the histograms. The absence of consistent systematic shifts in the mean of each histogram suggests that the majority of measured asymmetries are caused by random aerosol gradients.

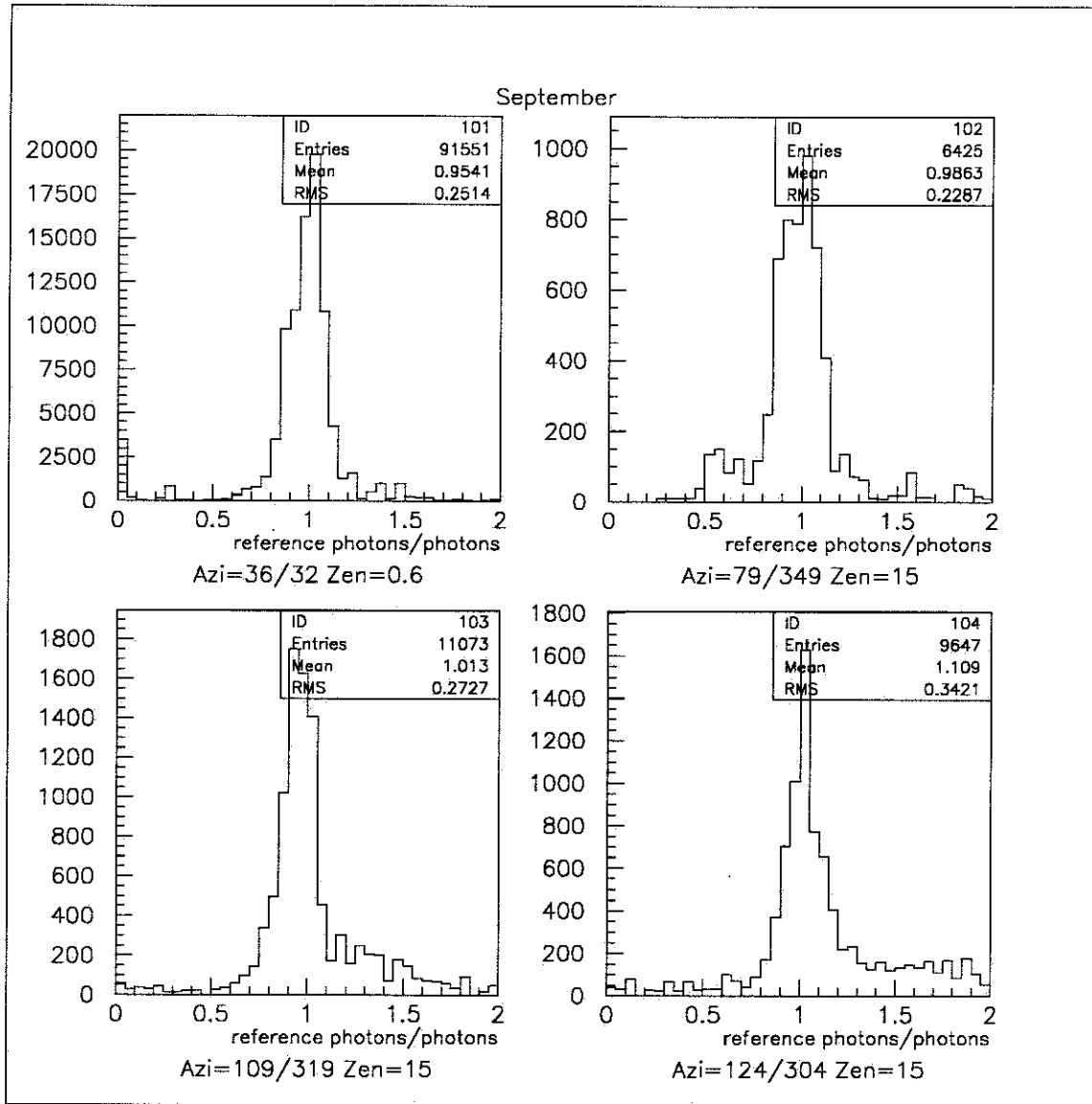


Figure 21: September data: Laser shots 2° either side of the detector are pictured in the first panel. The other three panels show shots taken at a zenith angle of 15° . The laser geometry is listed below each panel. Notice that the RMS deviation tends to increase as one moves further from the detector. All means are close to 1, suggesting a symmetric atmosphere.

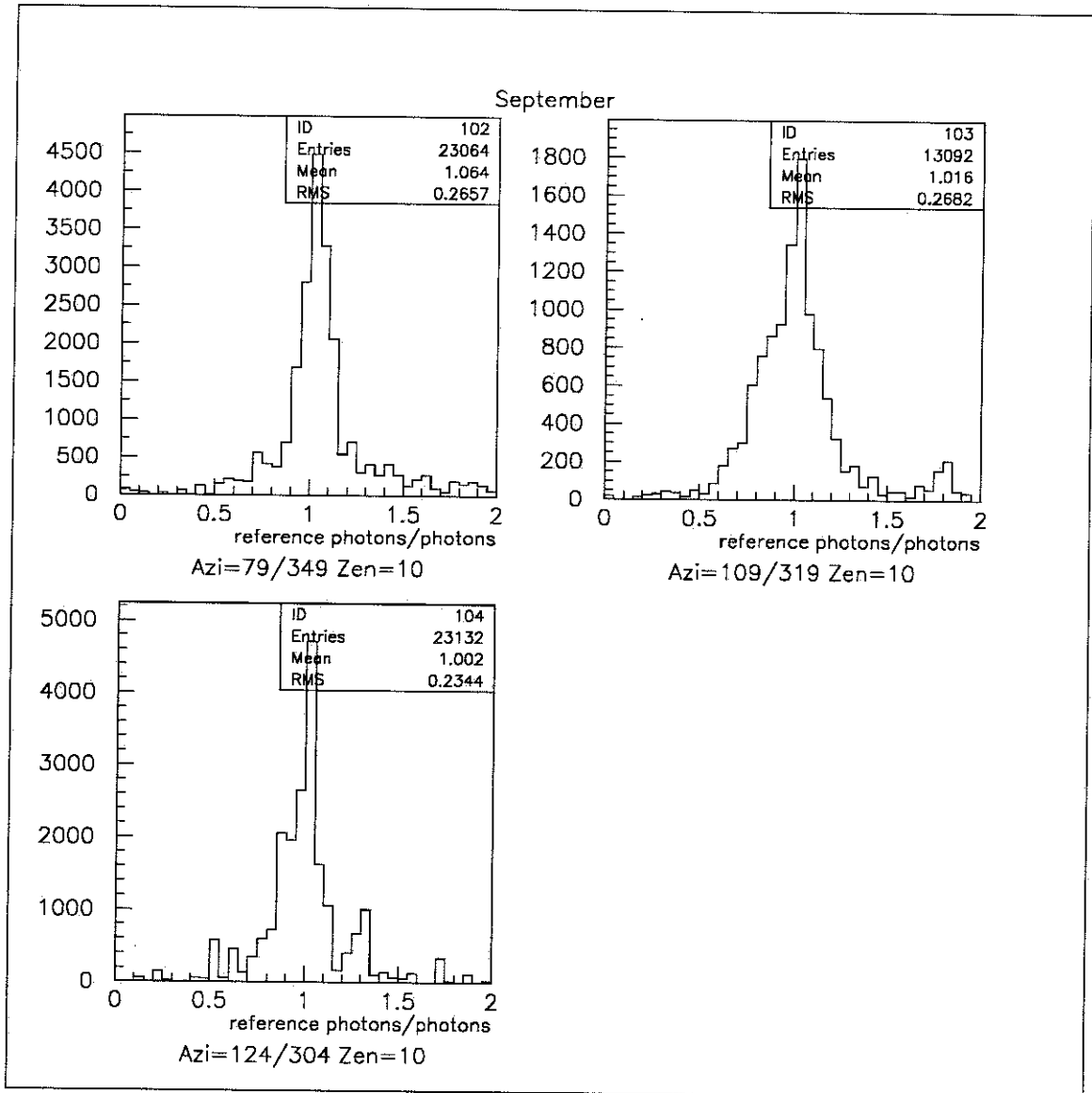


Figure 22: September data: Laser geometry is listed below each panel. This page shows shots that were taken at 10° elevation. Notice that the RMS deviation for these lower shots is greater than the corresponding deviation for the 15° elevation shots pictured on the previous page suggesting the presence of low-elevation asymmetric aerosols.

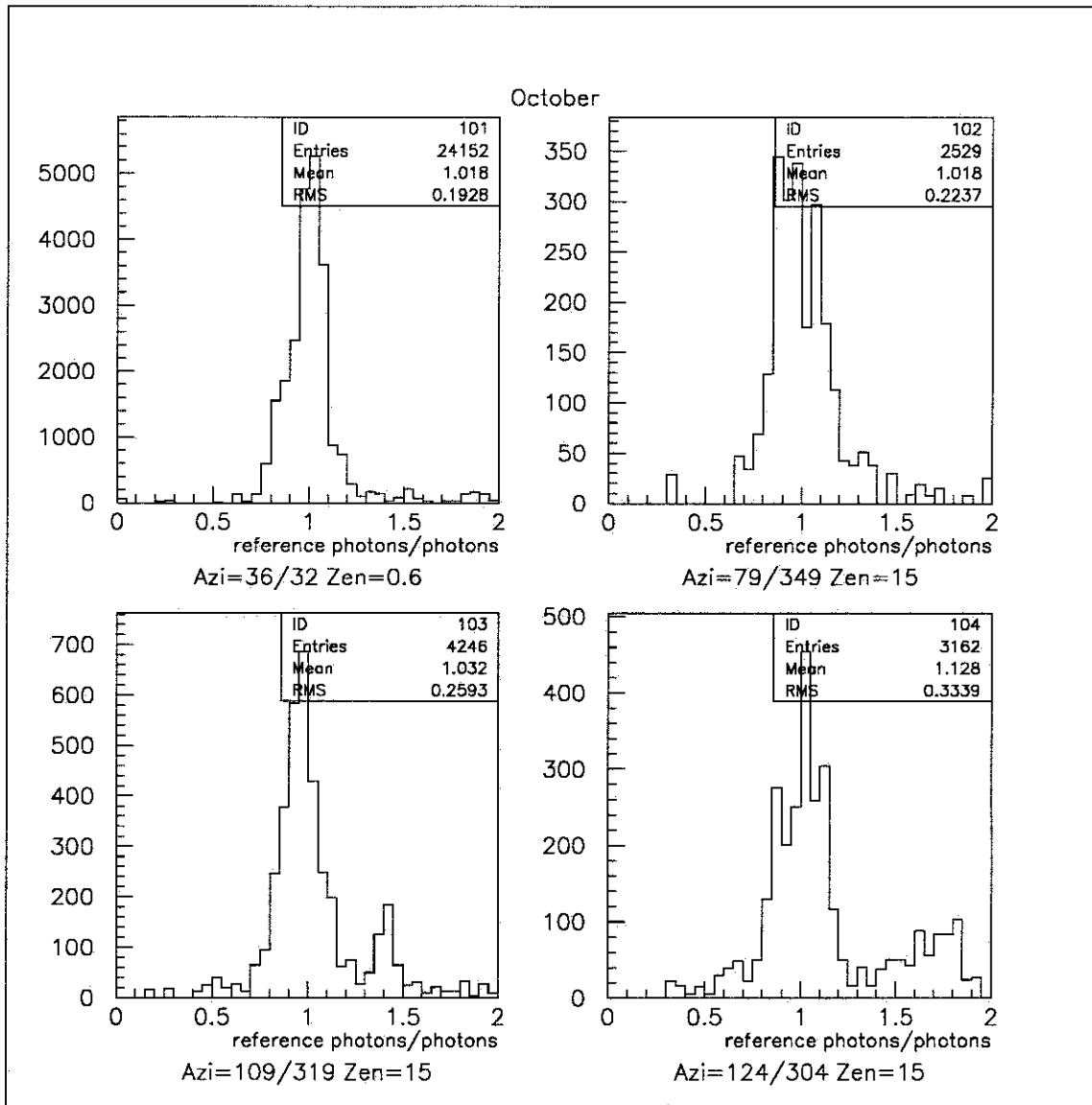


Figure 23: October data: Laser geometry is listed below each panel. Again, it appears that the RMS deviation increases as one moves further from the detector.

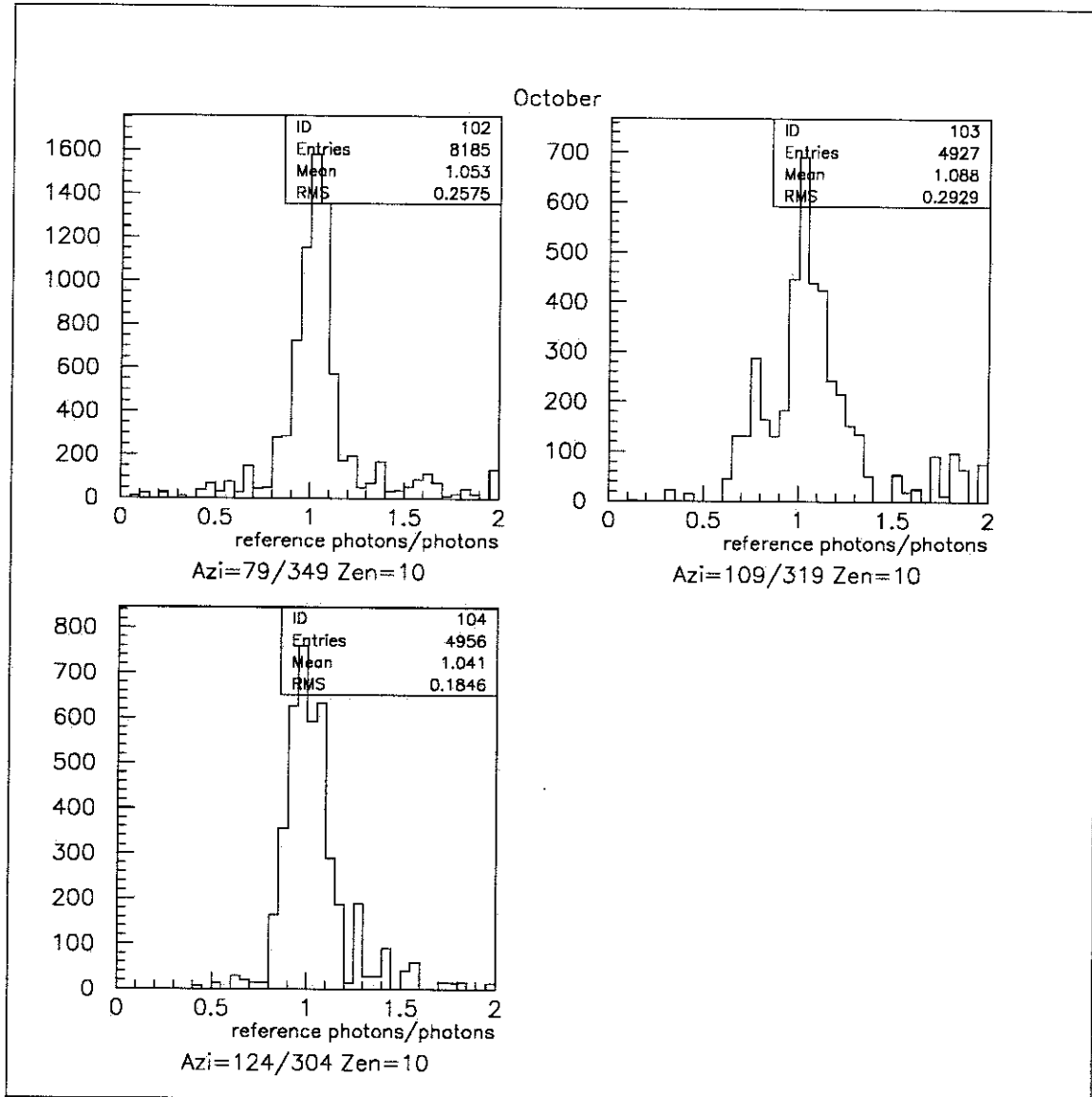


Figure 24: October data: Laser geometry is listed below each panel. Notice that the RMS deviation for the shots at 15° (previous page) are smaller than those for 10° (this page). This may indicate that there were high clouds scattering the shots with greater elevation angles.

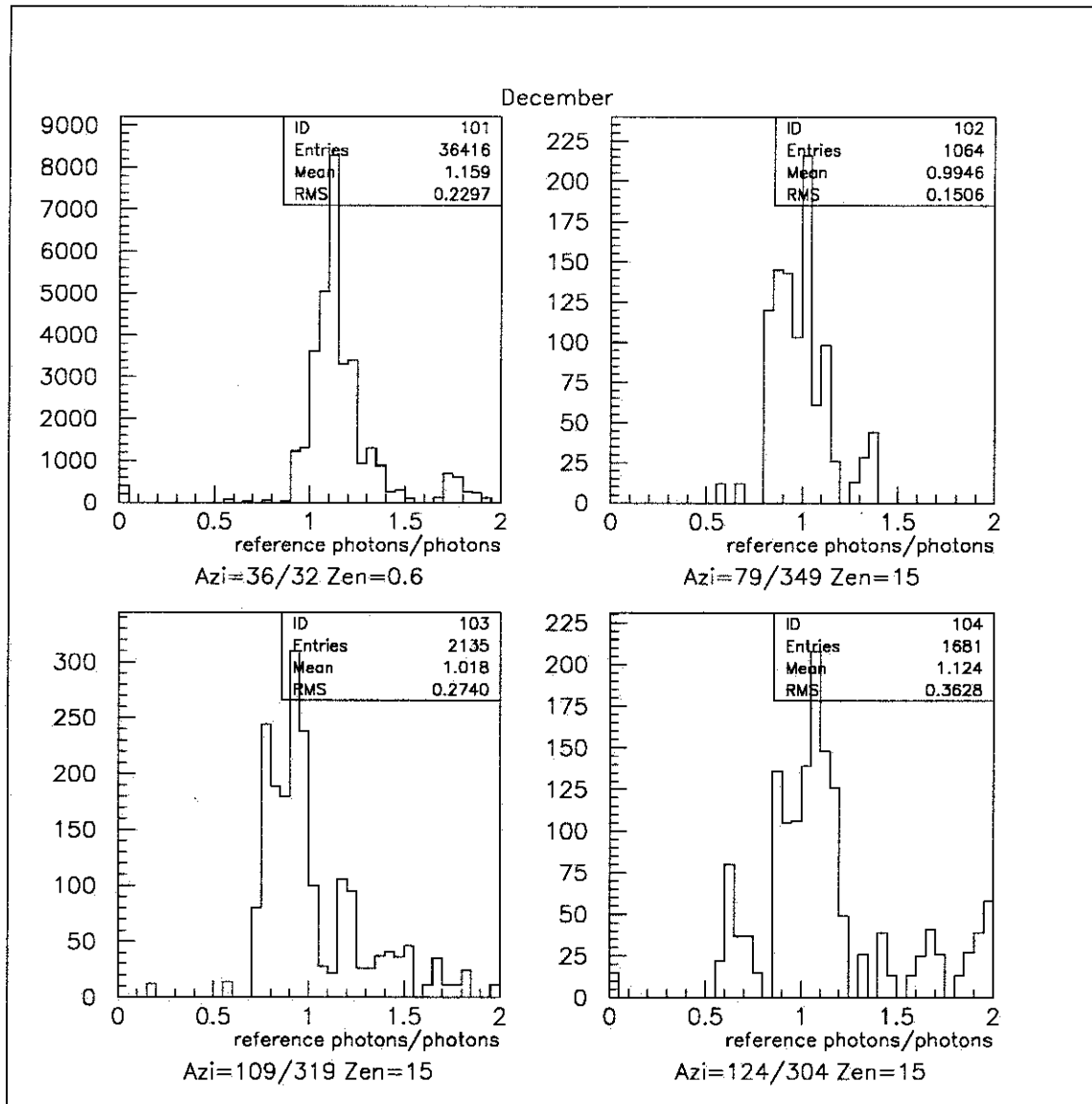


Figure 25: December data: Laser geometry is listed below each panel. The mean of the shots made at $\pm 2^\circ$ of the detector appears to have shifted indicating an asymmetry. In this case the South side of the detector measured a brighter signal than the North side when compared to the reference day. This is almost certainly not an atmospheric effect since the distance scale is so small. The reference day used to compare the data is from September. This offset mean may be an indication that the detector response changed between September and December.

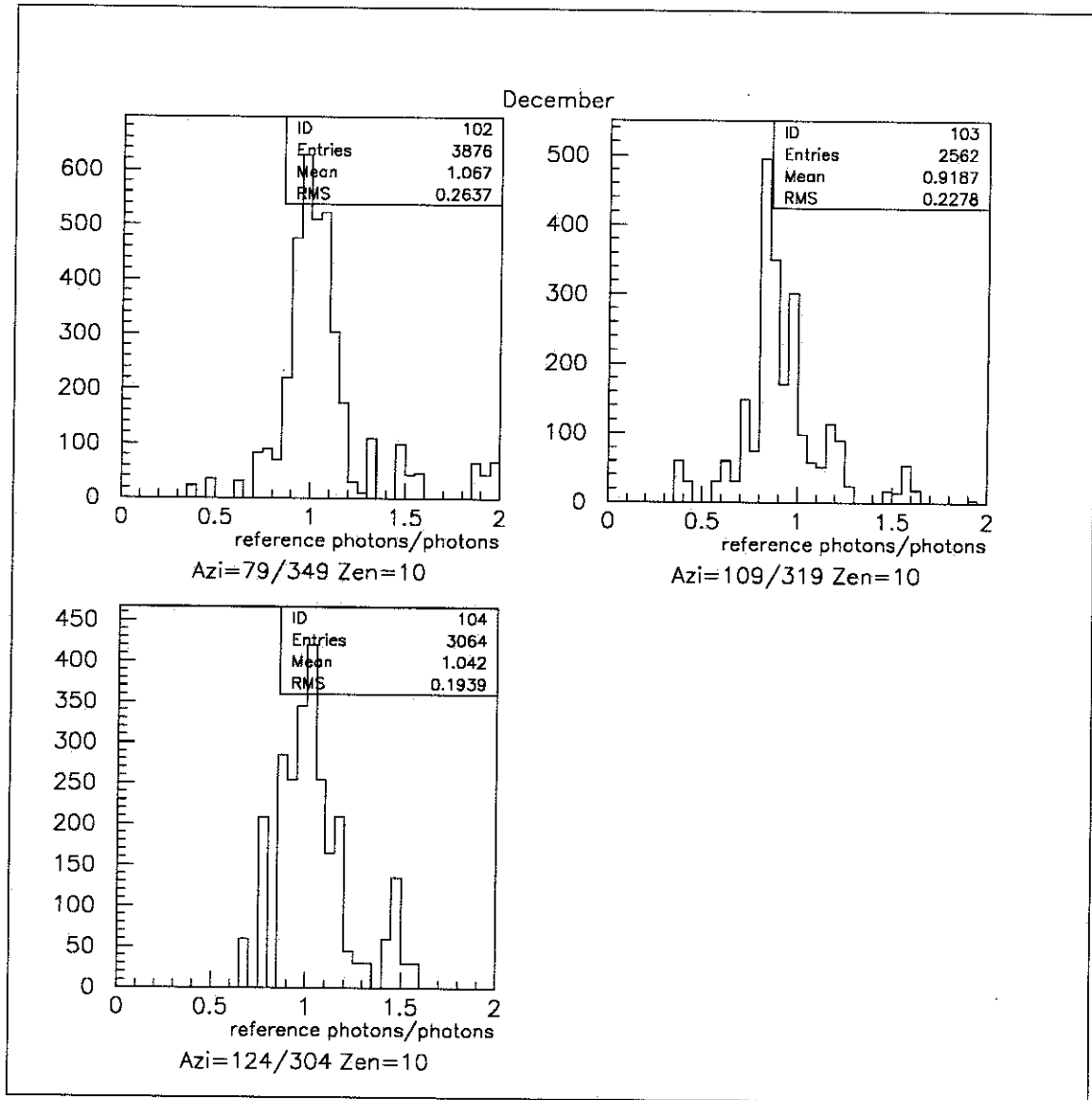


Figure 26: December data: Laser geometry is listed below each panel.

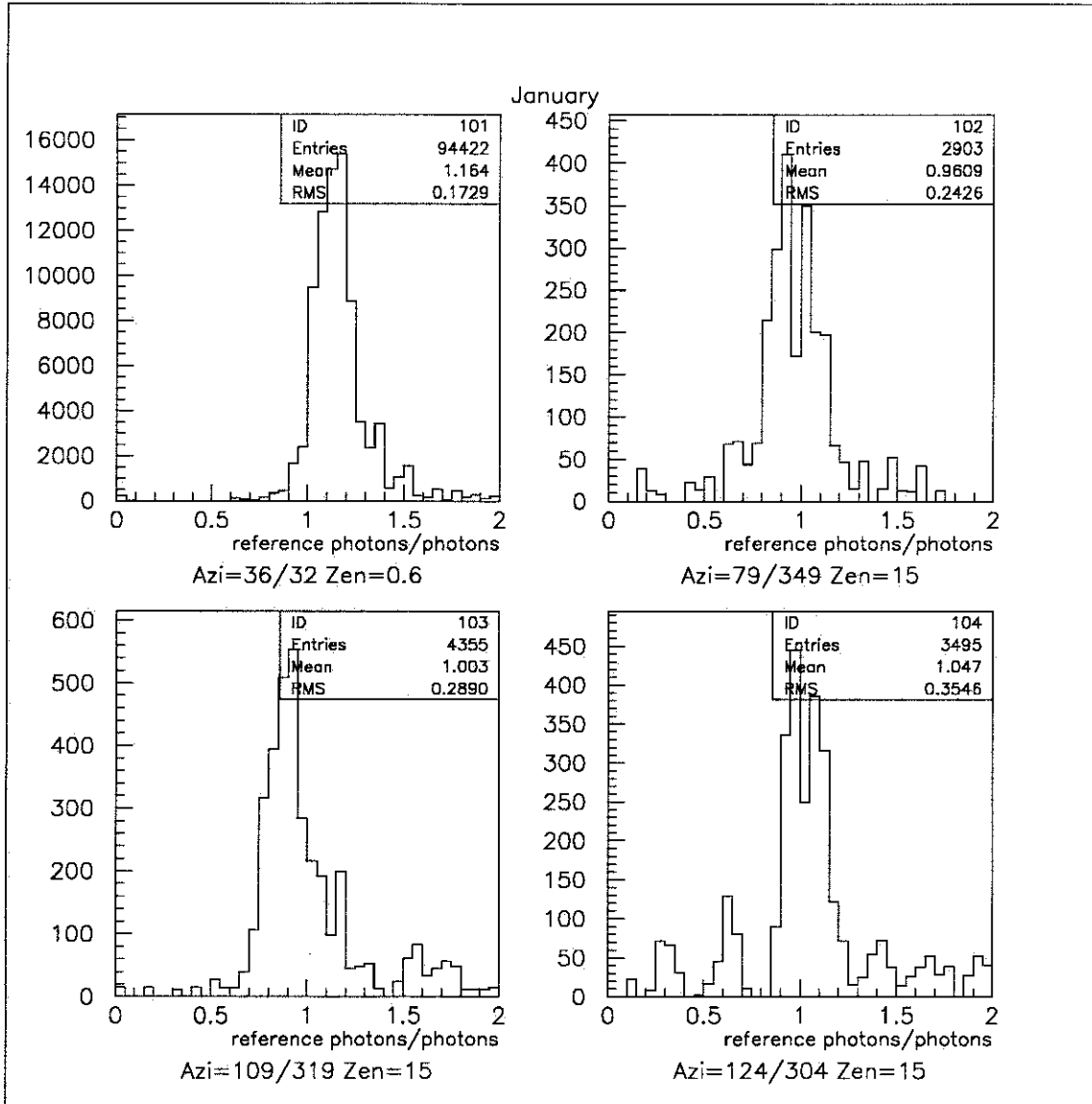


Figure 27: January data: Laser geometry is listed below each panel. Again, the $\pm 2^\circ$ distribution appears to show an asymmetry.

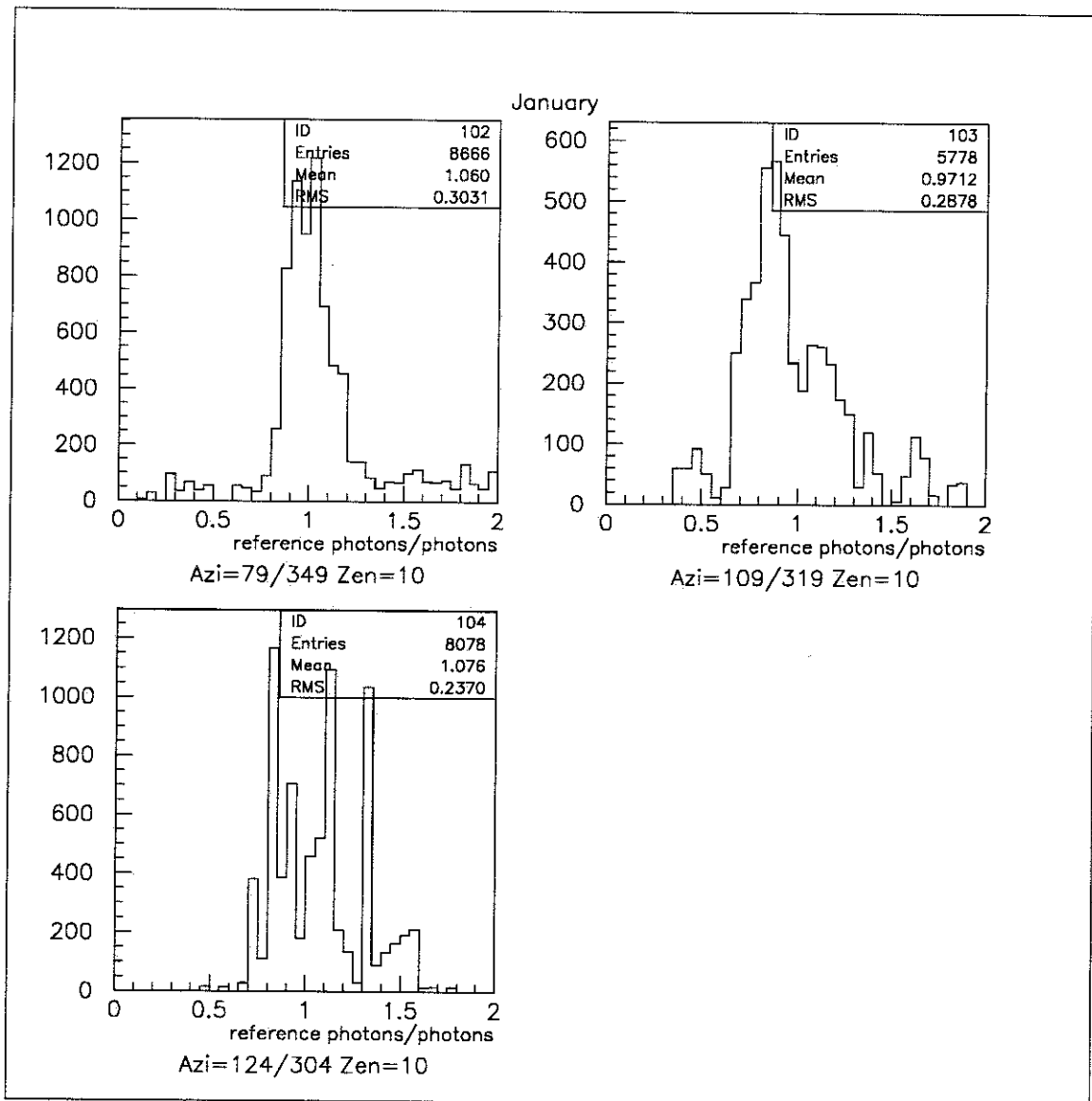


Figure 28: January data: Laser geometry is listed below each panel. These distributions suggest that January had one of the more symmetric atmospheres (at least for low elevations) in this data set.

7 CONCLUSION

The HiRes detector was used to measure light scattered from the HiRes 2 Steerable Laser System (HR2SLS) to measure atmospheric asymmetries. Asymmetries in both the HiRes detector and the HR2SLS were discussed and explored. Possible atmospheric asymmetries were isolated by normalizing measured laser shots to a reference day. This technique removes systematic asymmetries inherent in the detector and laser system. Atmospheric asymmetries were successfully measured and identified.

This is the first study of horizontal asymmetry at HiRes. It has been demonstrated that it is not always valid to assume that the atmosphere is horizontally uniform. The first conclusive measurements of atmospheric asymmetries were made. Over 100 hours of laser data, taken over 4 months, were studied. The largest measured asymmetry occurred in an atmosphere with a high concentration of aerosols. During this night, spatial asymmetries were measured that also changed with time.

When the concentration of aerosols decreases, the measured asymmetries also tend to decrease. However, fewer aerosols also reduce the sensitivity of the HiRes detector to horizontal aerosol distributions. In the limit that there are no aerosols, ie. a molecular atmosphere, we do not expect asymmetries that are large enough to be measured by HiRes. In near molecular atmospheres, or atmospheres with low aerosol concentrations, it is reasonable to describe the atmosphere with a one dimensional model, ignoring horizontal asymmetry. However, in atmospheres with high aerosol concentrations, horizontal asymmetries must not be ignored.

The lack of horizontal uniformity makes the task of modeling the atmosphere much more difficult. The traditional three-parameter model, that describes the atmosphere in terms of the ground-level extinction length, scale height, and mixing layer, is inadequate. A more complicated model, with parameters describing the horizontal distribution of aerosols should be developed.

In the four months of data examined, this study has found no conclusive evidence to suggest that systematic atmospheric asymmetries exist at HiRes. The lack of sys-

tematic asymmetries suggests that asymmetries are not dependent on the geography at HiRes but are more dependent on weather conditions such as wind and storm fronts. However, more data should be analyzed before the possibility of geographic dependent asymmetries are dismissed.

This study has been a survey of asymmetries at the HiRes detector. More data from the steerable laser needs to be examined before any conclusions are made concerning the symmetry of the atmosphere at HiRes. Within the next year, a second steerable laser system will be installed at HiRes 1 to be measured by the HiRes 2 detector. This new laser data, used in conjunction with the existing laser system, will provide much more data that will be invaluable for quantifying atmospheric asymmetries at HiRes.

A \mathcal{R} -PLOTS FOR SEPTEMBER 7, 1999

The plots included here are from three different geometries. All of the data in this appendix was taken on September 7, 1999 between the UT hours of 6 and 9. The geometries and hours are listed in the table below.

Figure #	Azimuth,Zenith	UT Hour	Comments
29	36°/32°, 0.6°	6	nearby laser shots
30	36°/32°, 0.6°	7	
31	36°/32°, 0.6°	9	
32	79°/32°, 10°	6	shots 45° either side of the detector
33	79°/32°, 10°	7	
34	79°/32°, 10°	8	
35	79°/32°, 10°	9	
36	124°/304°, 15°	6	shots 90° either side of the detector
37	124°/304°, 15°	7	
38	124°/304°, 15°	8	
39	124°/304°, 15°	9	

Laser shots at 79^{circ} and 349° azimuth are especially useful. An asymmetry is measured in both UT hours 6 and 7. By UT 8 and 9, the asymmetry has subsided and is much less prominent. See section 6.3 for a description of each panel in these figures.

Finally, we include 124/304 at 15 zenith shots too.

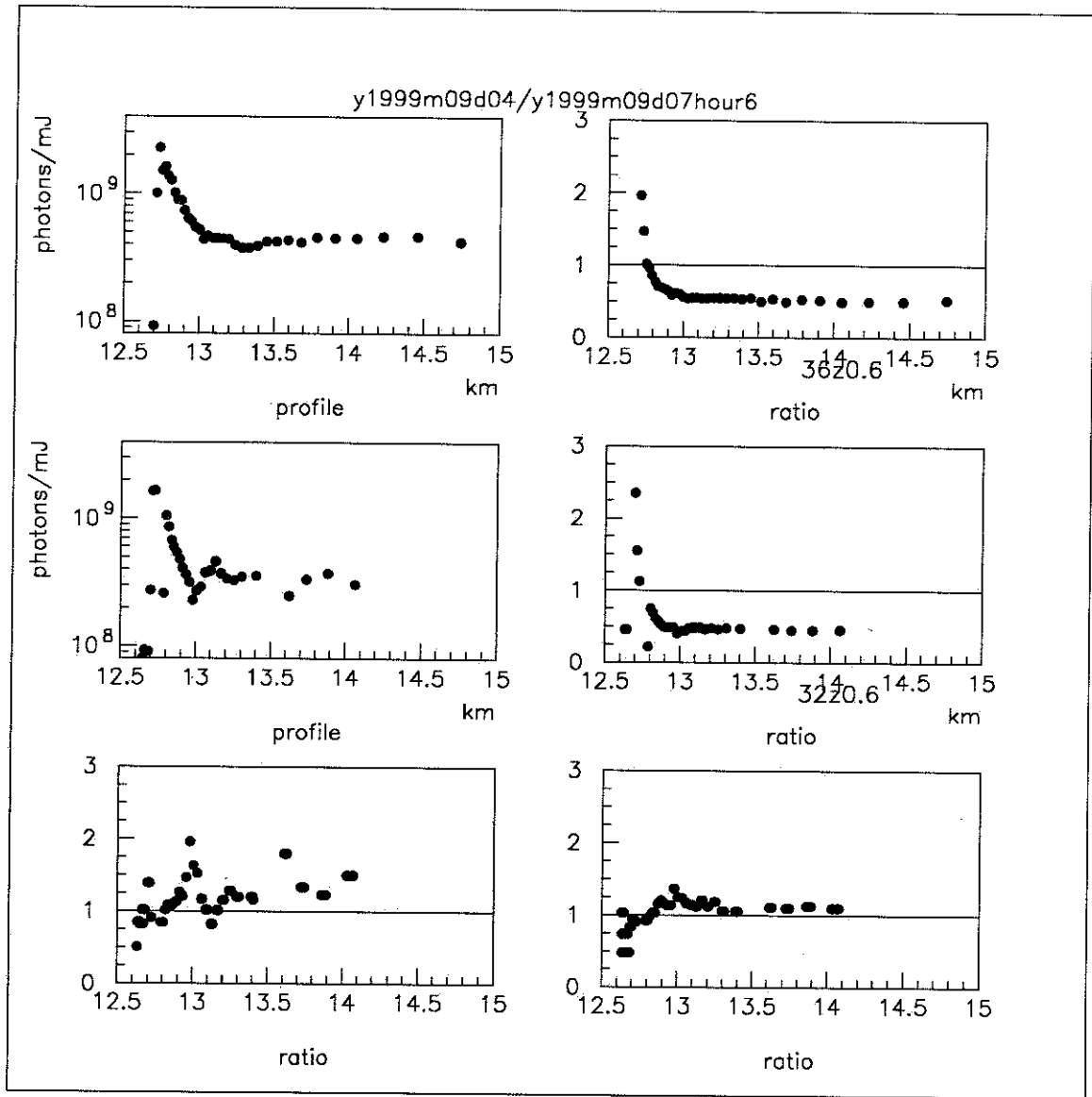


Figure 29: September 7, 1999; 6:00 UT. Azimuth angles of 36° and 32° at 0.6° elevation.

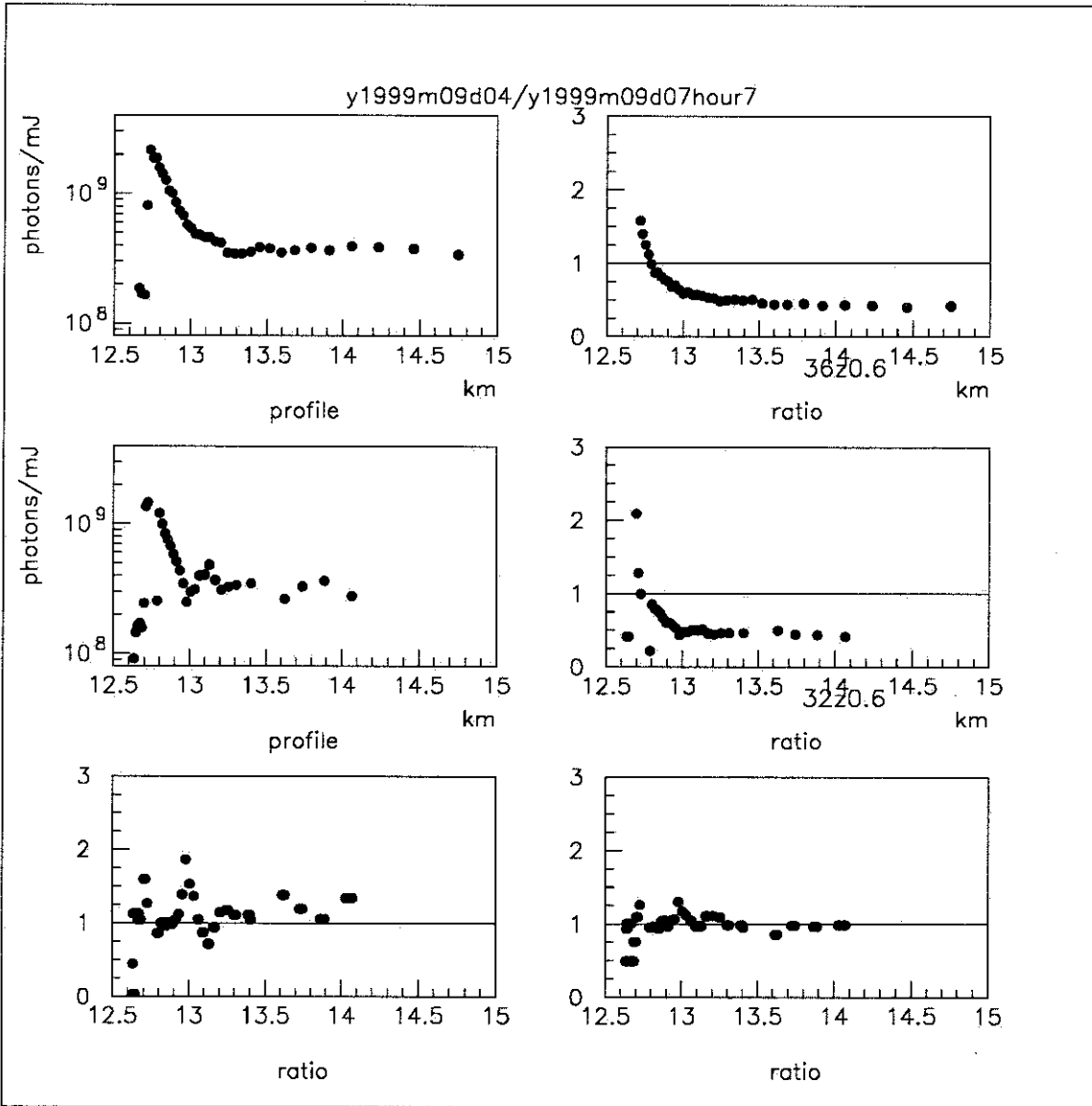


Figure 30: September 7, 1999; 7:00 UT. Azimuth angles of 36° and 32° at 0.6° elevation.

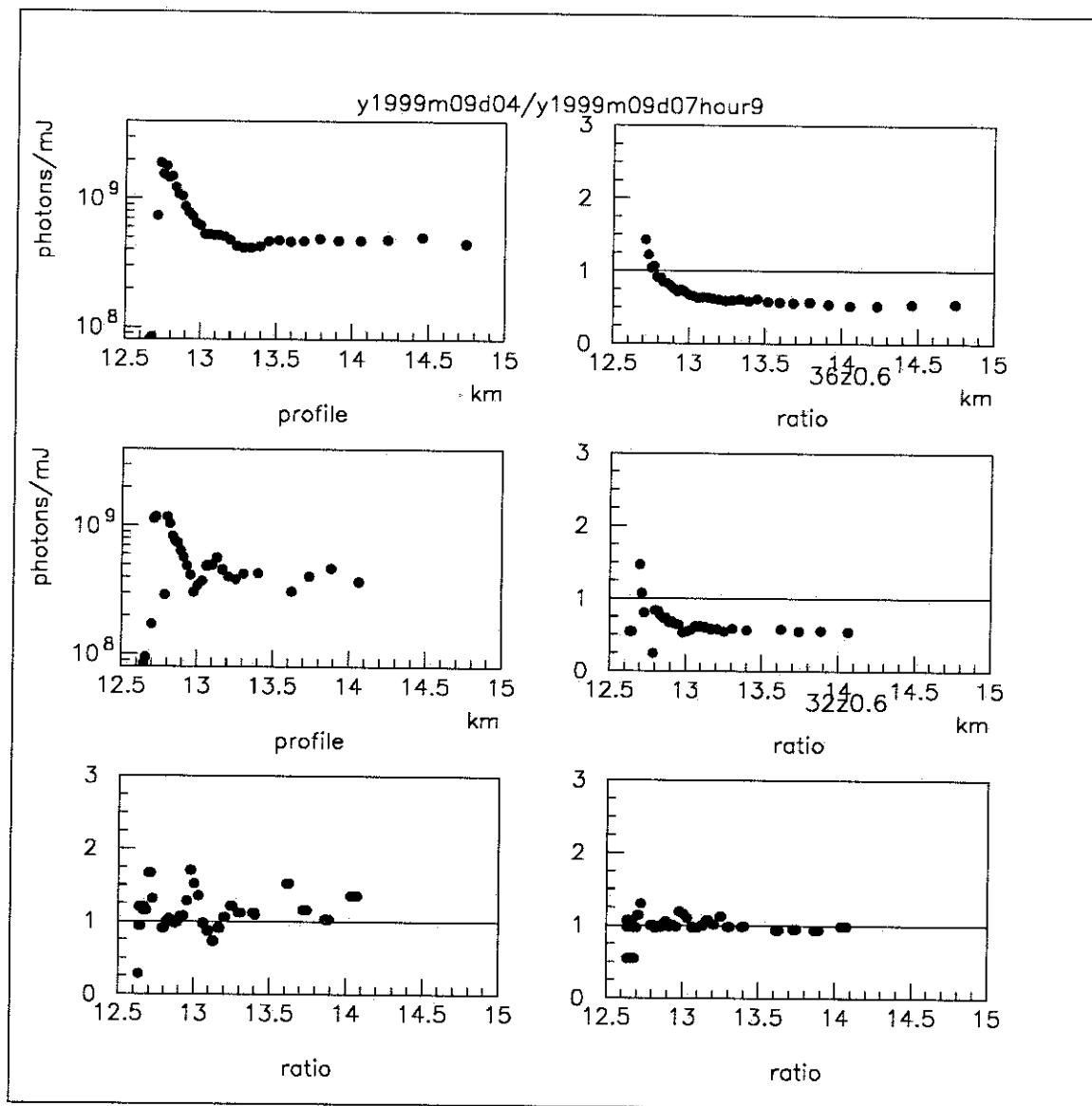


Figure 31: September 7, 1999; 8:00 UT. Azimuth angles of 36° and 32° at 0.6° elevation.

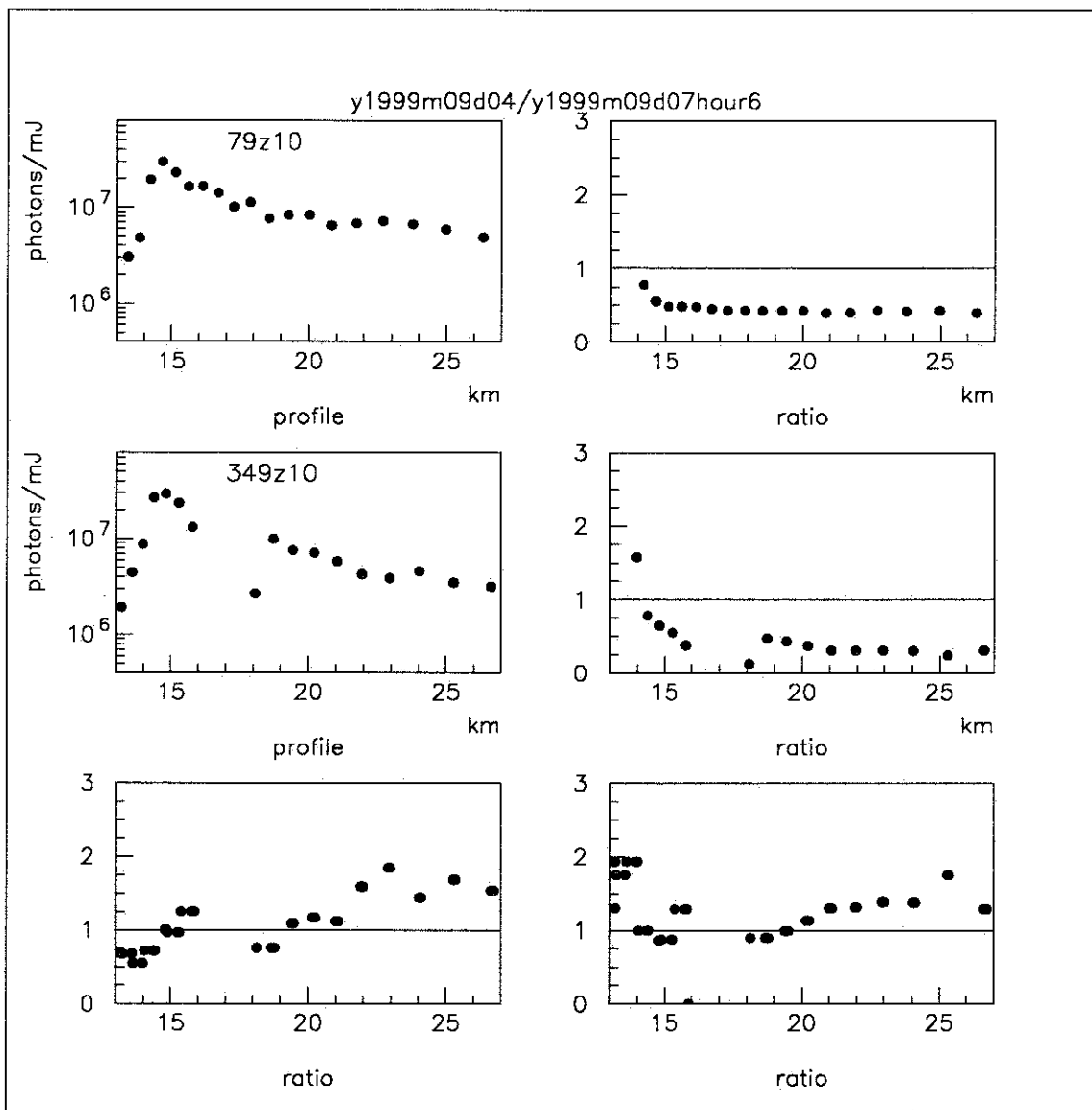


Figure 32: September 7, 1999; 6:00 UT. Azimuth angles of 79° and 349° at 10° elevation.

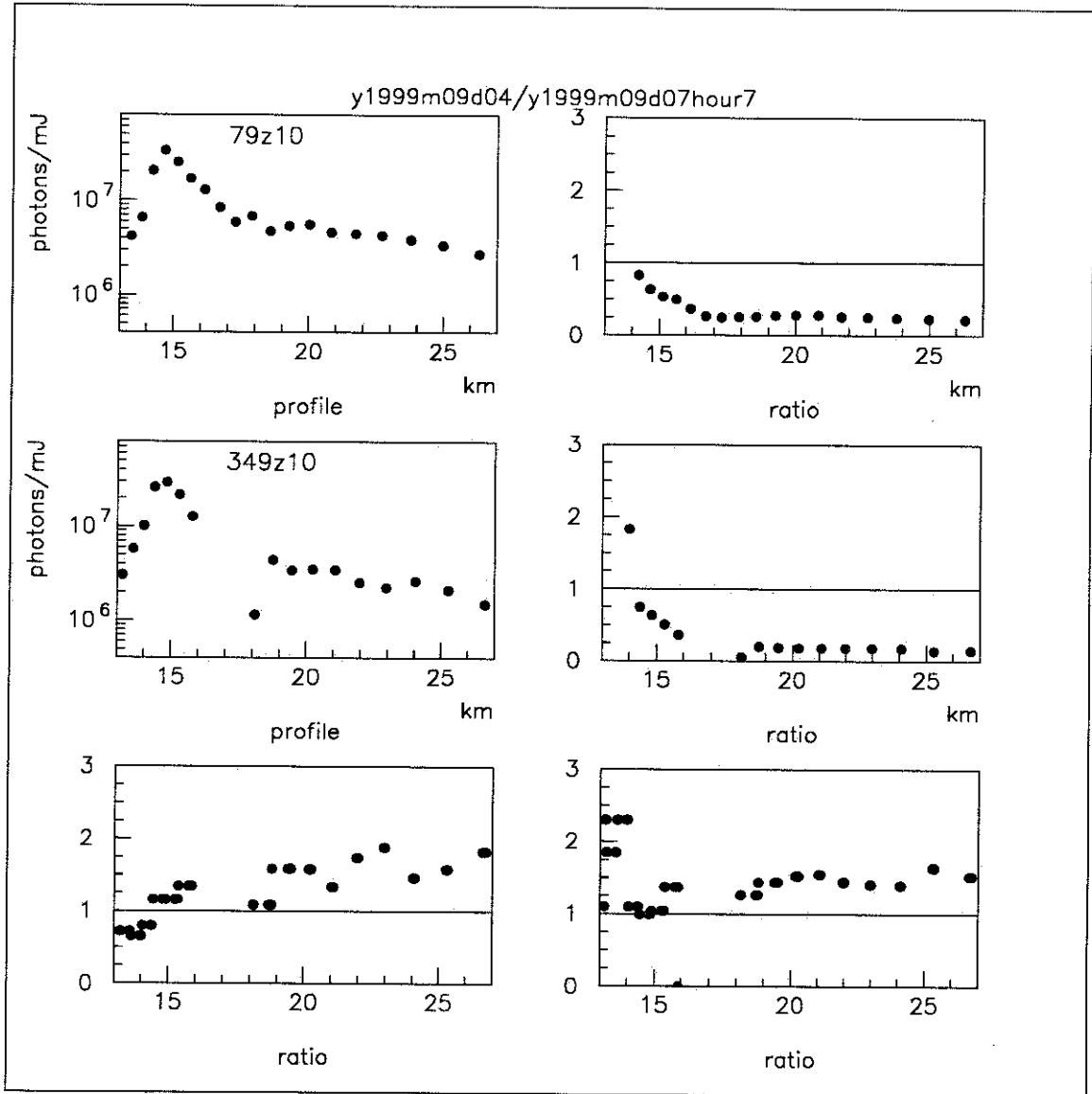


Figure 33: September 7, 1999; 7:00 UT. Azimuth angles of 79° and 349° at 10° elevation.

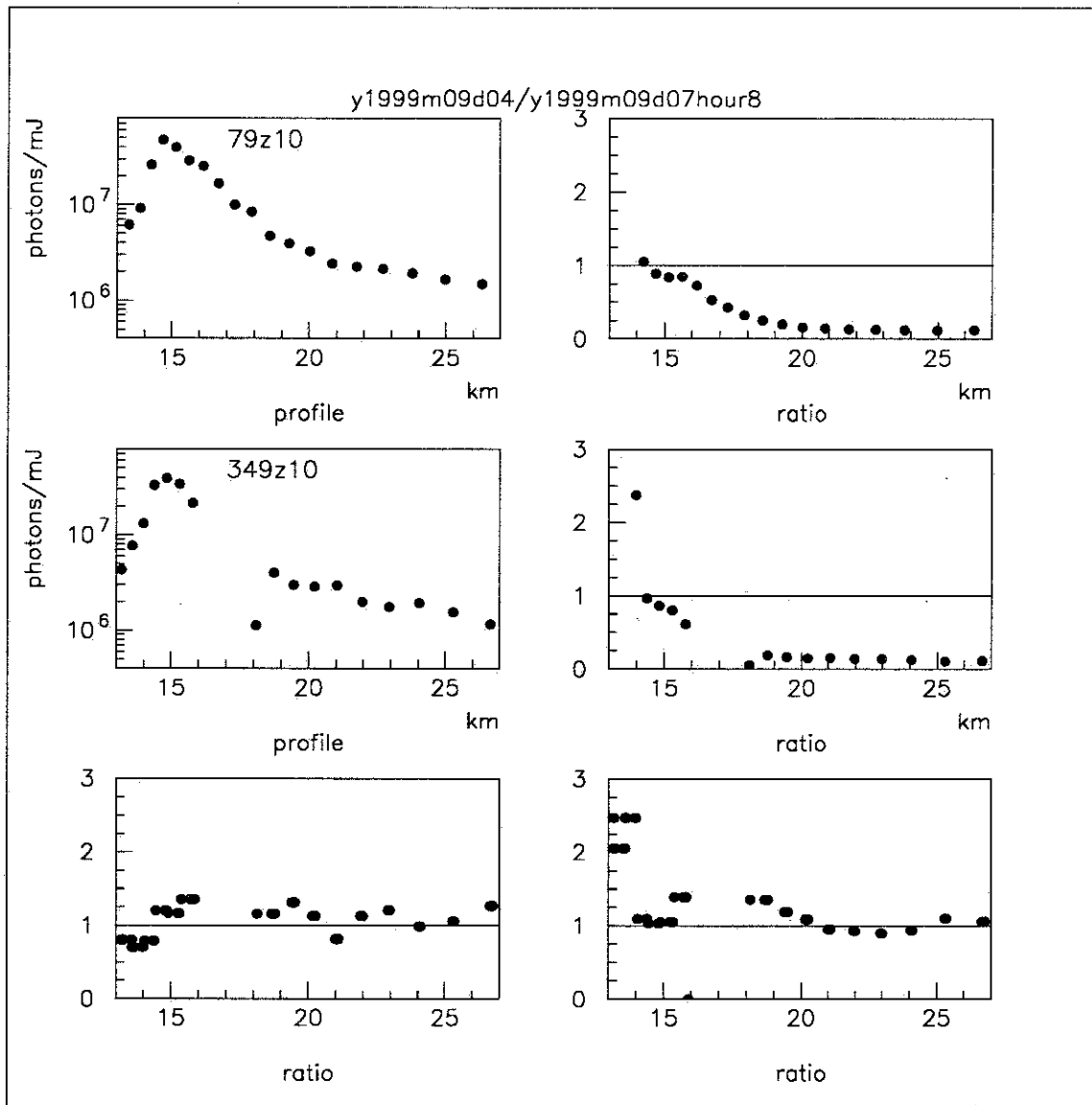


Figure 34: September 7, 1999; 8:00 UT. Azimuth angles of 79° and 349° at 10° elevation.

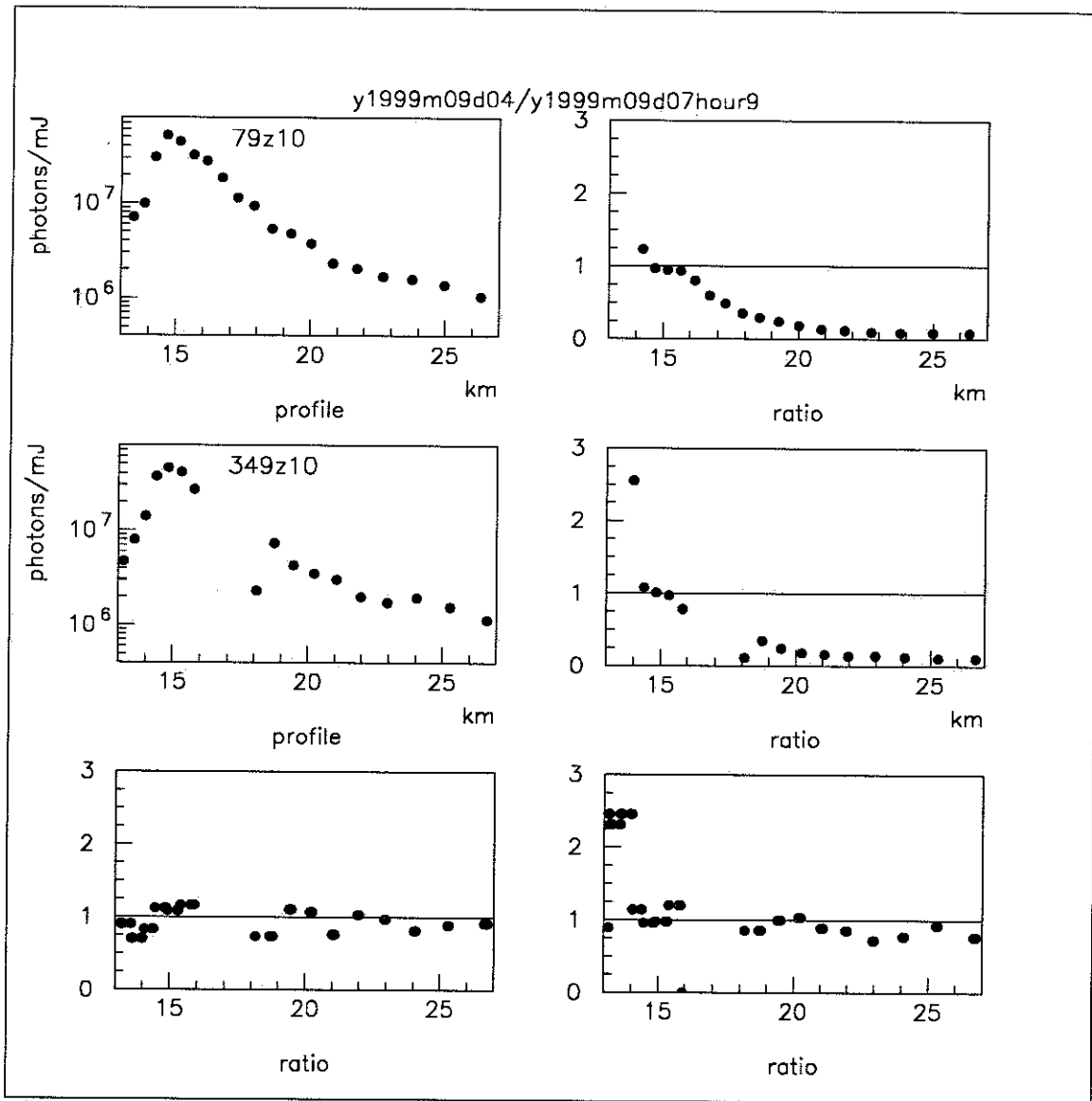


Figure 35: September 7, 1999; 9:00 UT. Azimuth angles of 79° and 349° at 10° elevation.

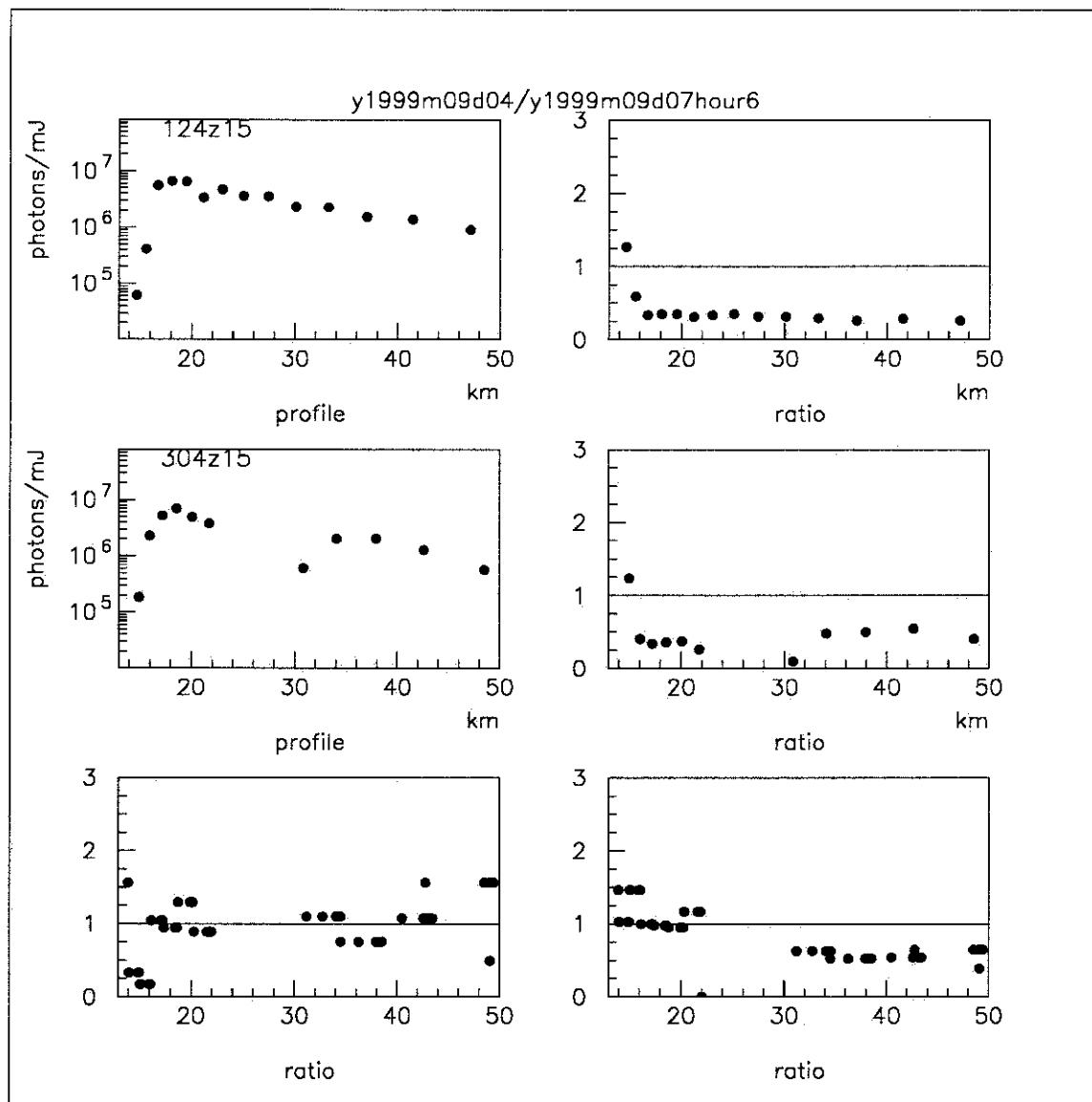


Figure 36: September 7, 1999; 6:00 UT. Azimuth angles of 124° and 304° at 15° elevation.

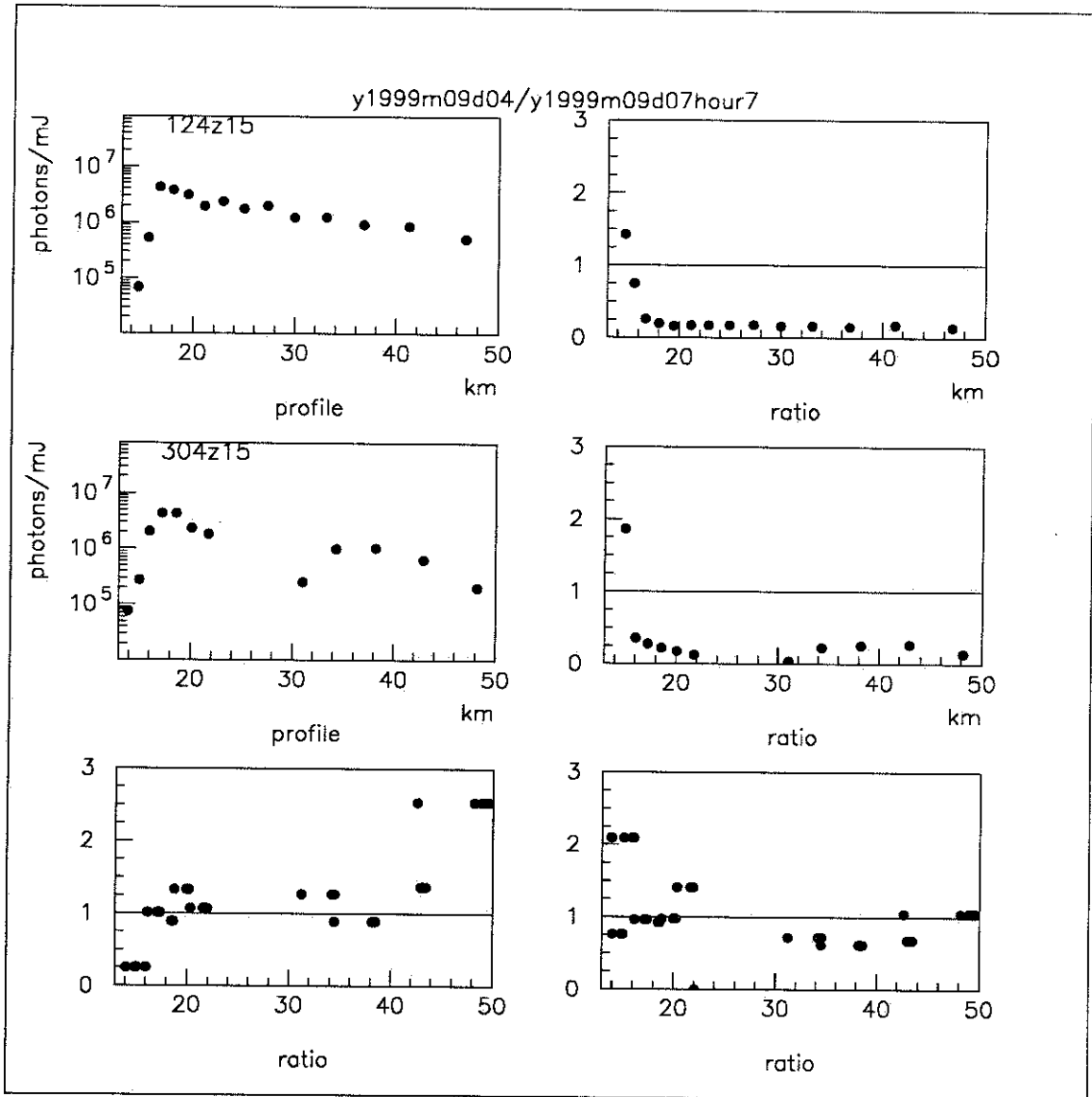


Figure 37: September 7, 1999; 7:00 UT. Azimuth angles of 124° and 304° at 15° elevation.

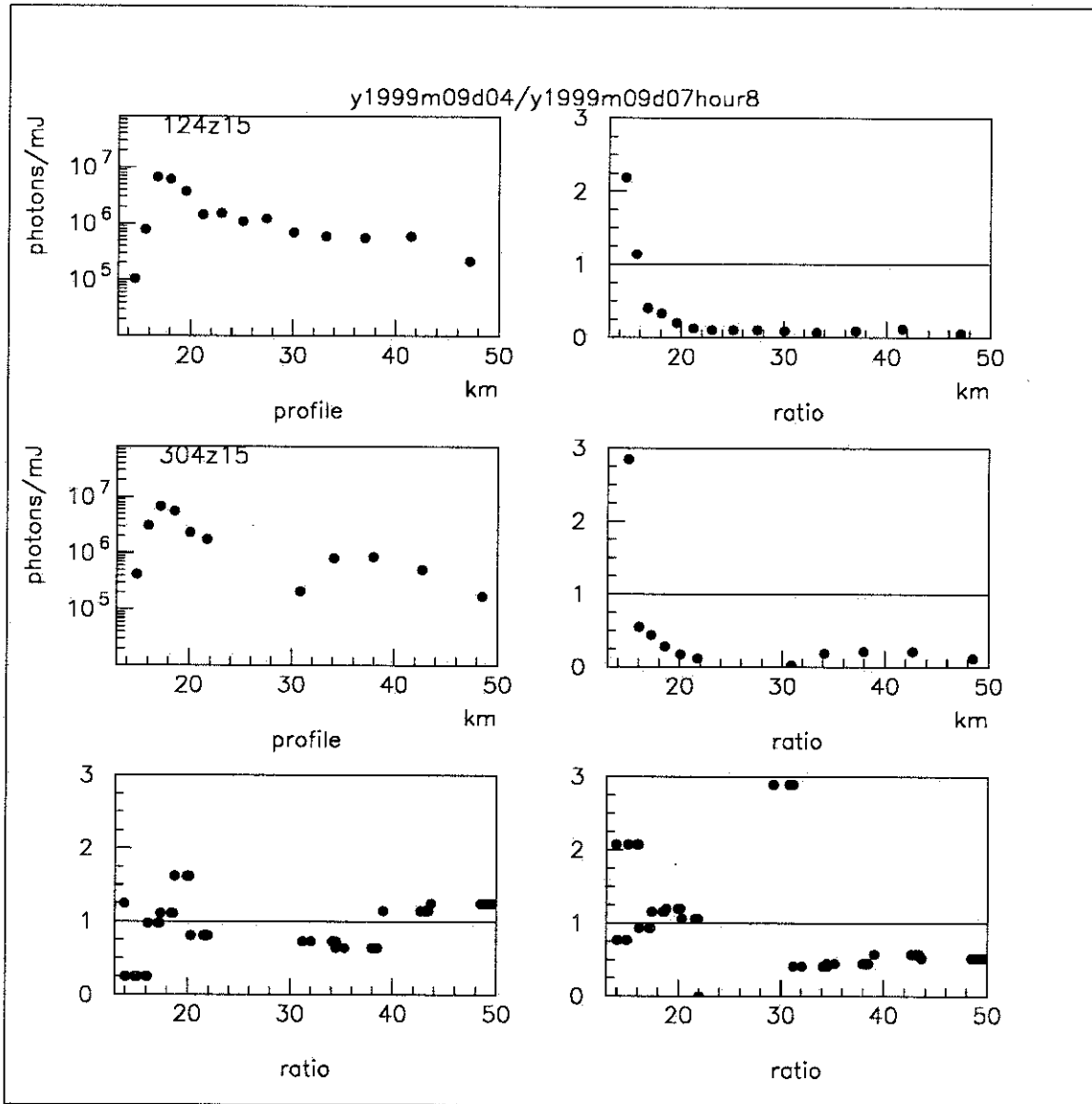


Figure 38: September 7, 1999; 8:00 UT. Azimuth angles of 124° and 304° at 15° elevation.

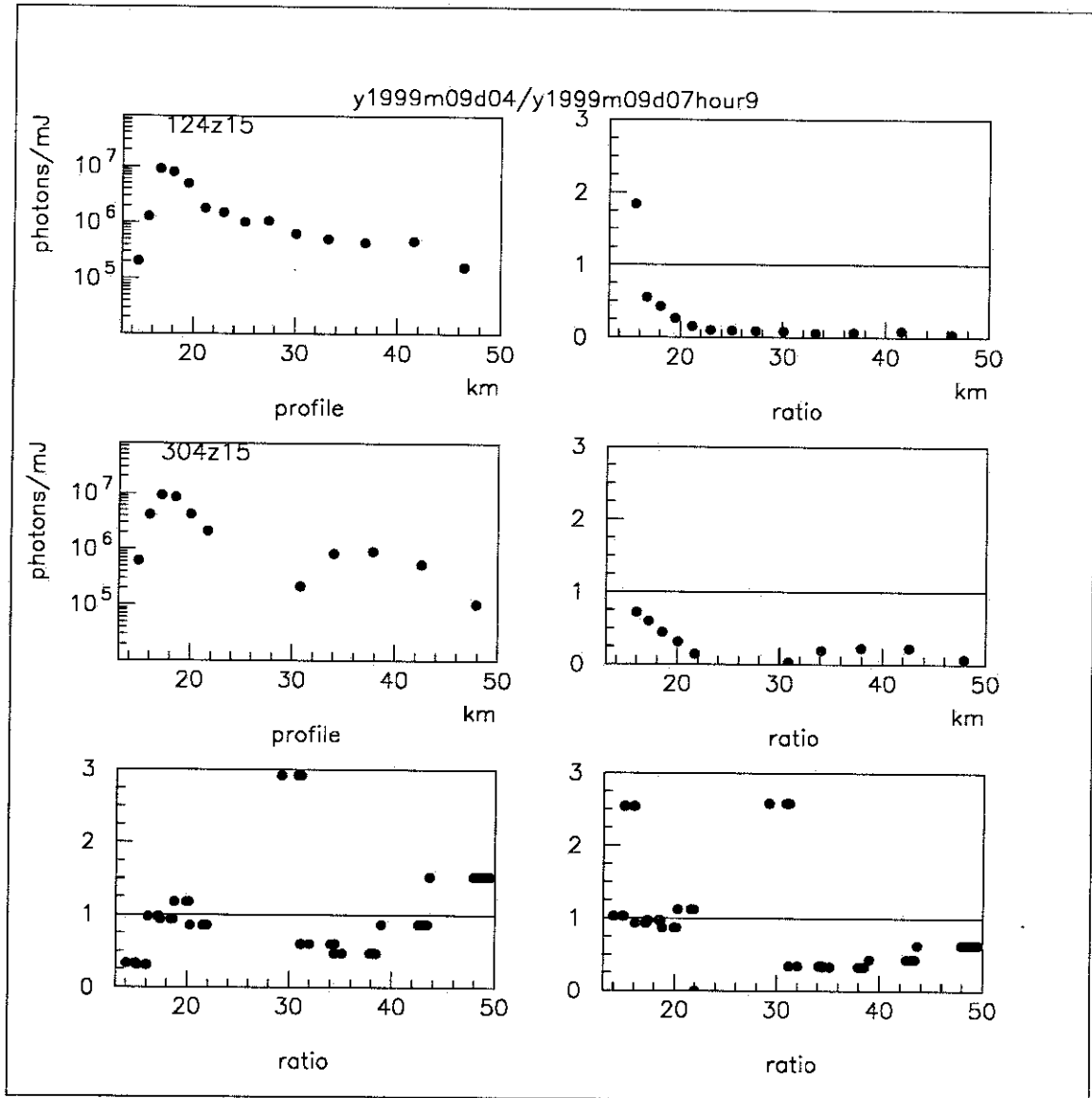


Figure 39: September 7, 1999; 9:00 UT. Azimuth angles of 124° and 304° at 15° elevation.

B AUTOMATIC LASER SUMMARY REPORTS

The HR2SLS is consistently monitored to ensure that the laser continues to function properly. An important part of the monitoring is an automatically generated report created each night that the laser is run. A short description of the automatic summaries, taken from the summary web-page,³ follows.

HTML Summary Help Page

This page is meant to serve as a general summary of the information that is reported in the automatic nightly html-based HR2SLS reports.

General Information(*see figure 40*)

- **Operator** Lists the initials of the operator or operators that logged into HR2SLS to run the system.
- **Login Time** Lists the time that the operator logged into HR2SLS.
- **Summary File** Lists the file that was used to create the summary. The summary file is of the form: yYYYYmMMdDDp00.hr2sls.autolog. This "p00" autolog file is a compilation of all autolog files generated in a given run night. This "p00" file is deleted after this summary page is created. See the "Autolog File Summary" for a complete list of autolog files generated in a given night.

Loop Summaries

The loop summaries table lists several characteristics of each loop that was run during the night. Most of the parameters are self explanatory. There are however a couple of items to notice.

³<http://teddy.physics.utah.edu/users/atmos/summary/gifs/summryhelp.html>

- **Incomplete Loops** Incomplete loops are flagged with an asterisk in the table. An incomplete loop is any loop that was ended prematurely, before the loop had completed itself automatically. An incomplete loop is the result of one of the following: an operator issued a "stop" or "restart" command, or the system crashed or was not shut down properly while a loop was running.
- **Average Energy** The average energy listed here is the average energy of all of the shots that were fired during this loop hour that were measured (ie. greater than or equal to zero). This calculation of average energy ignores shots that were not properly measured by the monitor probe. The average energy listed was measured by the monitor probe and is not multiplied by any constants including: filters, Esky numbers, or any other external constants. This is just the raw number from the radiometer.

Big Sky Ultra Laser Statistics

The first part of this section is a plot showing all of the energies of shots as a function of UT hour. There should generally be a highly populated band of shots for all of the hours that the laser was operated. There may also be small patches of lower energy shots that are possibly due to a different voltage setting on the Big Sky Ultra laser. Again, the energies listed here are the energies as measured by the Monitor Probe.

In addition to the plot for the current night, a plot is generated to monitor the laser output energy as a function of total operating days. The average energy of all of the shots fired in a given night are plotted versus the Julian day. The current plot shows the average energy of the laser over a span of about 500 days. This laser energy vs. time plot helps to evaluate the overall energy output of the laser. figure 42 shows that the laser energy dropped dramatically at the Julian day of about 10900. the laser was repaired and reinstalled.

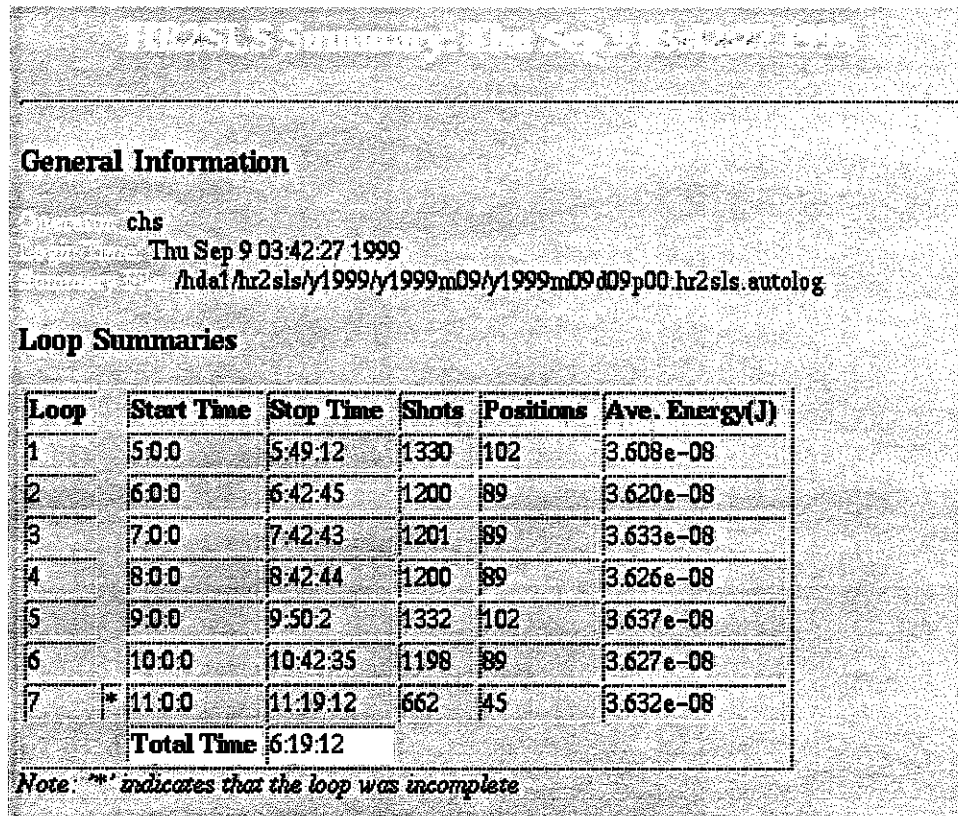


Figure 40: Sample automatic summary report.

The next section lists laser statistics in a table. This plot breaks the laser shots into five categories

1. Normal Energies
2. Intermediate Energies
3. Low Energies
4. No Measured Energy
5. All Measured Energies

All of these energies are parameters specified in the header file:

`$cbuvm/sumry/lsr_stats.h,`

on lidarpc.hires2.utah.edu, and can easily be changed.

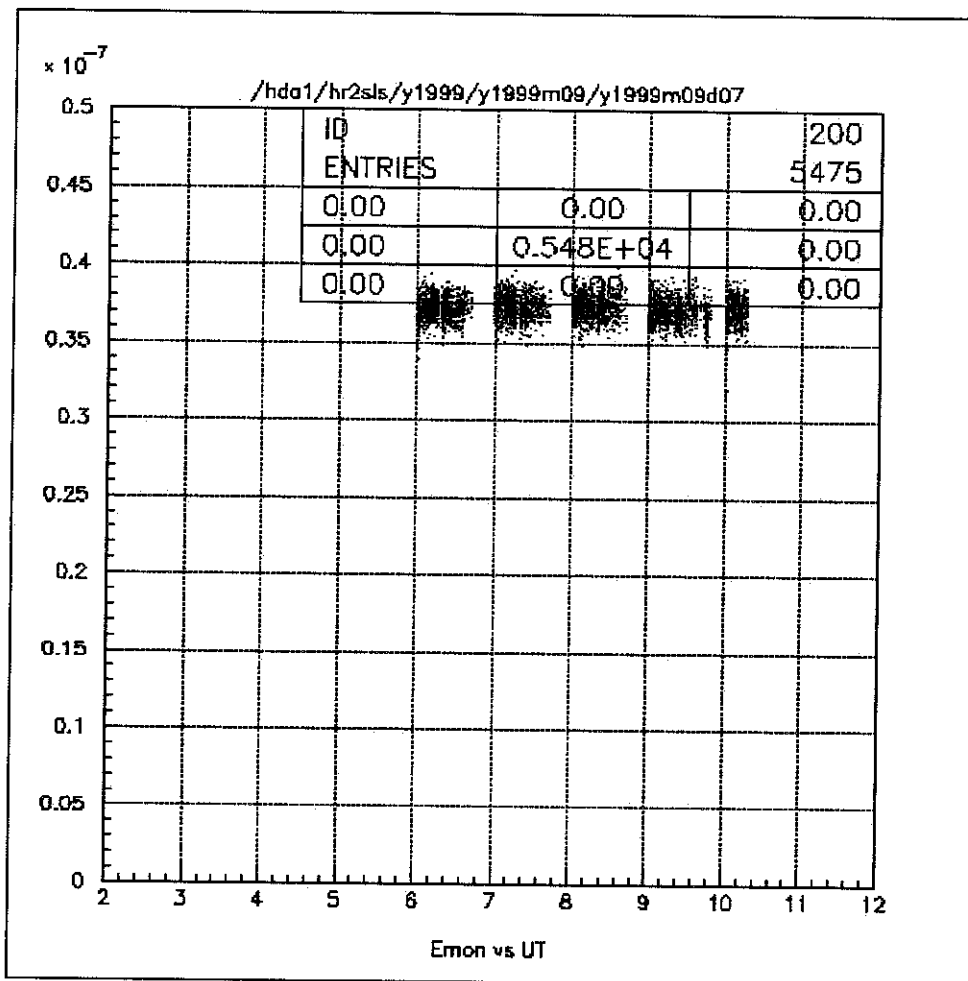


Figure 41: Monitor probe energy as a function of UT hour.

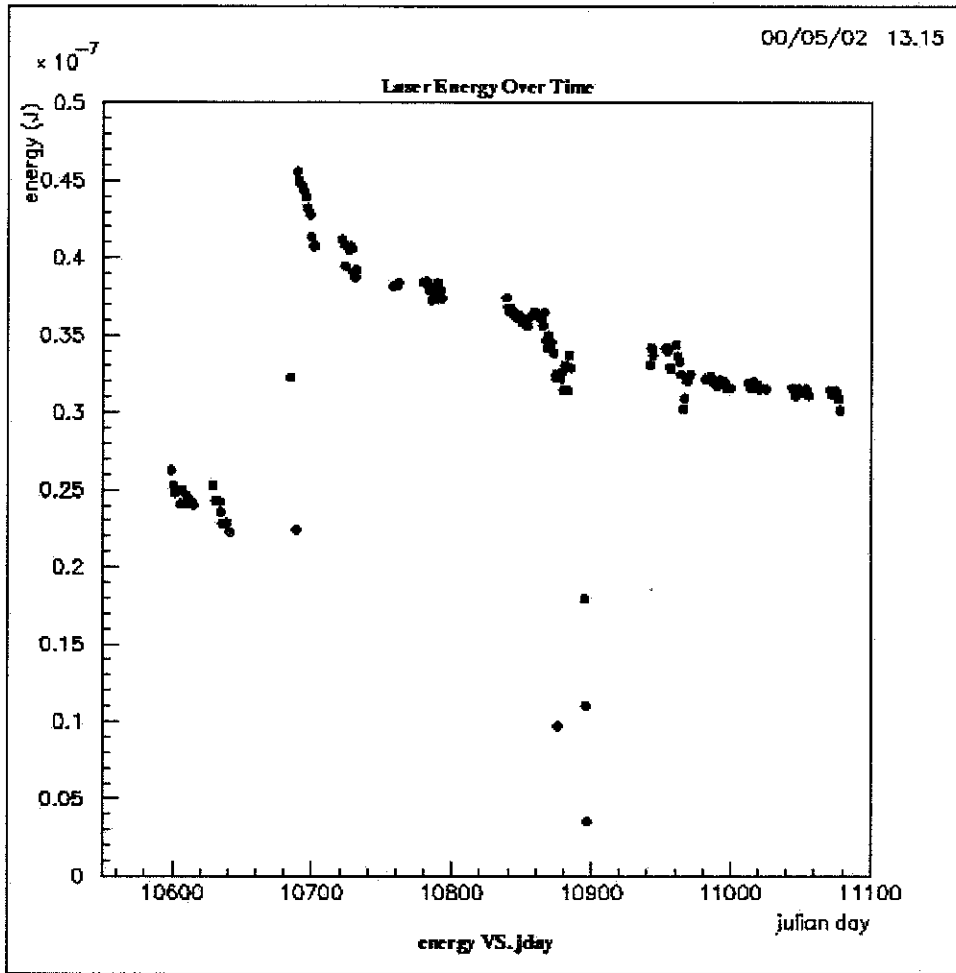


Figure 42: Total average laser energy plotted versus Julian day. Although the laser energy is dropping, it appears to be stabilizing since it was reinstalled in December 1999 (around Julian day 10940).

For each energy region listed in the table, the mean energy is computed and the standard deviation from the mean is also calculated and reported as a percent. The total number of shots for each bin is also reported.

The "No Measurement" bin records all of the shots that reported to be -9.999e9 by the radiometer in the autolog file for the night. No average or standard deviation are reported for these shots.

The next plot is a four panel set of histograms designed to give a graphical representation of the information displayed in the previous table (*see figure 43*).

The histograms are the following:

1. The upper left corner is a histogram of all of the laser shots that were measured to be greater than or equal to zero. Again, we expect that there will be one large peak showing the energy of the laser shots during the normal operations mode of the laser. Smaller peaks may be due to adjustments that were made to the laser volatage and flash bulb settings.
2. The upper right corner is a histogram that zooms in on the laser shots classified as "Normal Energy". Again, this is a parameter that can be changed by modifying the `lsr_stats.h` file on lidarpc. The average and standard deviation are reported for the "Normal Energy" shots in upper right corner of the plot.
3. The lower left corner is a histogram that zooms in on the shots classified as "Intermediate Energy". This plot helps to flag any below-par performance of the Big Sky Ultra laser.
4. The lower right corner is a histogram of all of the shots that are very near zero. This plot should normally be empty. If this plot begins to show data, it might suggest that there is a problem with the laser operation or the monitoring of the laser energy.

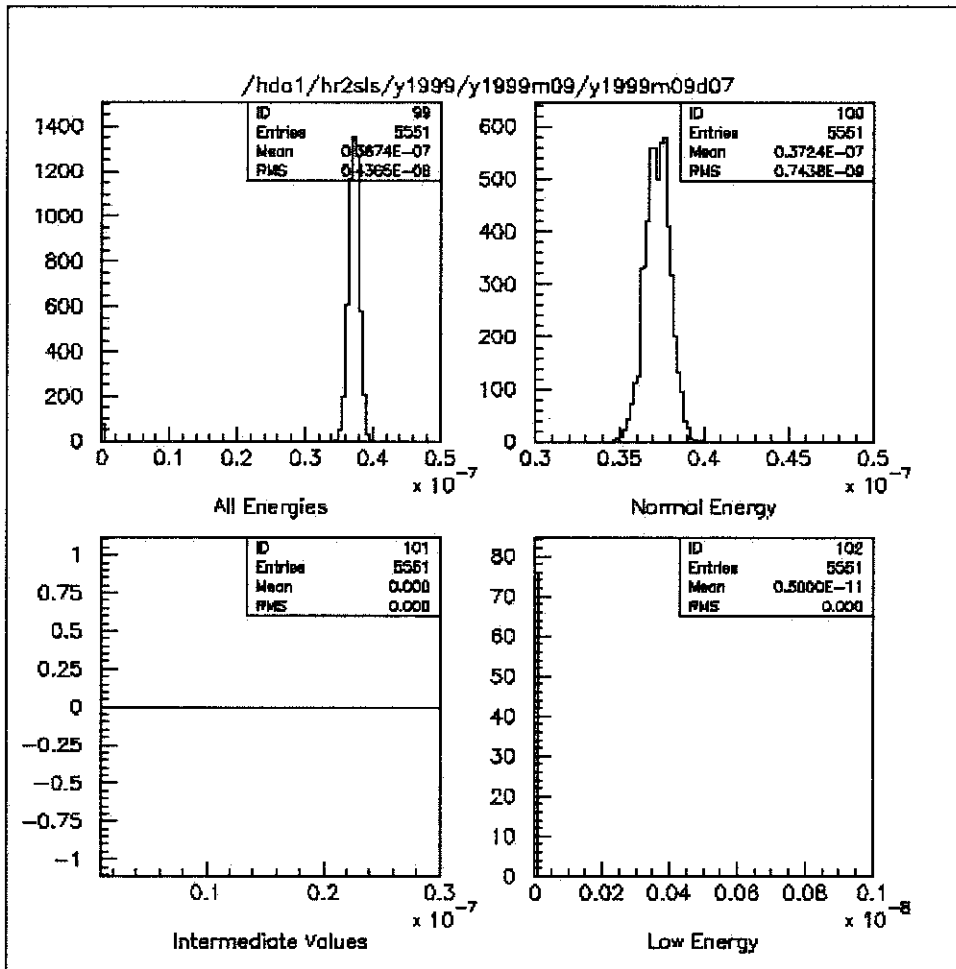


Figure 43: Plots that monitor the performance of the laser over different energy regions.

Operator Commands

This section of the report lists all of the commands issued by the operator while running the HR2SLS laser system (*see figure 44*). Each entry lists the command issued and the time. The commands listed are pulled from all of the autolog files created during the night.

Warning Summary

This section is similar to the Operator Command summary in that it searches all of the created autolog files for all of the Warnings that are produced when HR2SLS is issued a "diag" command. Warnings that you might see are the following:

- **DIAG:WARNING:HAL:not connected to Hal.** Lidarpc has not established a network connection with Hal. If Lidarpc is not connected to Hal, commands may not be issued from Hal to HR2SLS.

If all went as planned and there were no warnings to report, "No Warnings to Report" will be displayed in this field.

Autolog File Summary

The Autolog file summary is a link to a text file listing all of the autolog files generated on a given night. The text file lists the size of the autolog files in bytes and their location on Lidarpc.

Conclusion

Each night that the laser is run, a message will be mailed to a mailing list of those parties that are interested in keeping an eye on the operation of the laser system. The mail message will be short, reminding the receiver that the laser was operated the previous evening. Included in the body of the message will be the location of the html summary file.

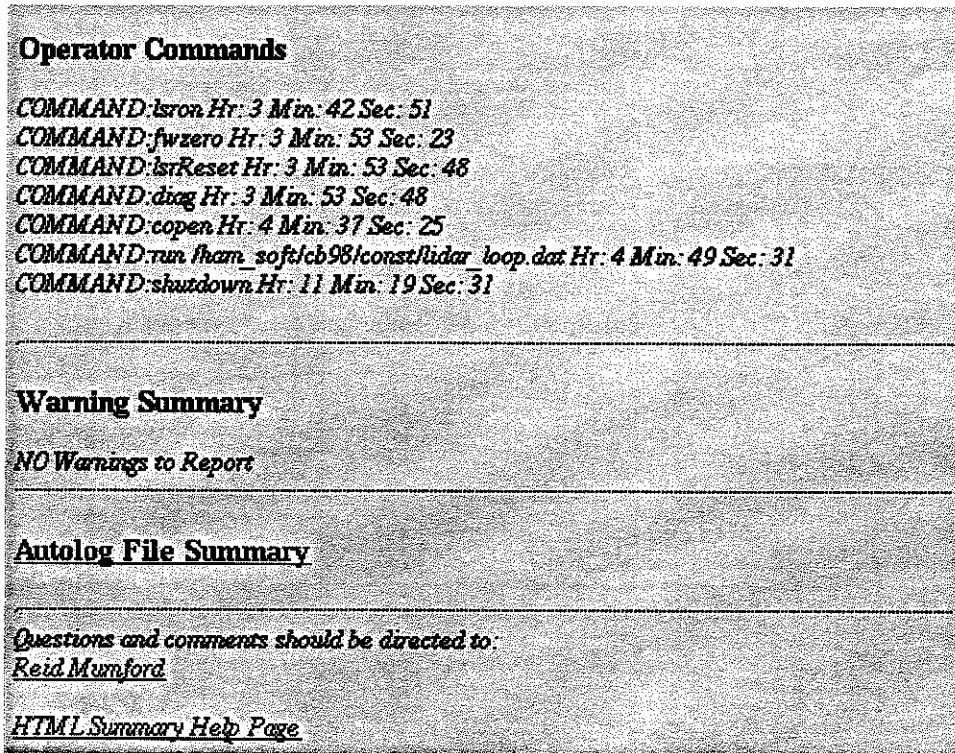


Figure 44: Commands issued by the operator during the night of laser operation.

REFERENCES

- [1] Thomas G. Kyle, *Atmospheric Transmission Emission and Scattering* (Pergamon Press, 1991).
- [2] David R. Longtin, *A Wind Dependent Aerosol Model: Radiative Properties* (AFGL-TR-88-0112, April 1988).
- [3] *Handbook of Chemistry and Physics, 79th Edition* (ICRC Press, 1998), p. 14-10.
- [4] Air Force Research Laboratory: MODTRAN Software Download.
<http://www-vsbn.plh.af.mil/soft/modtran.html>
- [5] F. Kakimoto *et al.* Nucl. Instr. and Meth. A 372 (1996) 527.
- [6] R.C.Gray, Senior Thesis, University of Utah, 2000, *Extracting Aerosol Parameters for the High Resolution Fly's Eye Using Bistatic LIDAR with Multiple Scattering Corrections.*
- [7] Big Sky Lasers. Model: CFR Ultra (frequency trippled)
<http://www.bigskylaser.com>
- [8] J.R. Mumford *et al.* in *26th ICRC* (Salt Lake City, 1999), OG 4.5.10, Vol. 5, p. 377.
- [9] R.C.Gray *et al.* in *26th ICRC* (Salt Lake City, 1999), OG 4.5.04, Vol. 5, p. 353.
- [10] D.R. Bergman *et al.*, *HiRes Mirror Positions from GPS Surveying*. September, 1999.
- [11] B.F. Jones *et al.* in *26th ICRC* (Salt Lake City, 1999), OG 4.5.25, Vol. 5, p. 429.
- [12] G. Martin *et al.* in *26th ICRC* (Salt Lake City, 1999), OG 4.5.06, Vol. 5, p. 361.
- [13] G.L. Martin *et al.*, *Analysis of Time Variant Molecular Atmosphere for the Purpose of Air Fluorescence Measurements*. October, 1999.

- [14] T.Z. Abu-Zayyad, Ph.D. thesis, University of Utah, 1999.
- [15] R.A.R Tricker, *Introduction to Meteorological Optics* (American Elsevier Publishing Co, Inc, 1970).

Name of Candidate: Jonathan Reid Mumford
Birth Date: May 22, 1976
Birth Place: Salt Lake City, Utah
Address: 2011 Pheasant Way
Salt Lake City, UT 84121